HHS Public Access

Author manuscript

Sci Immunol. Author manuscript; available in PMC 2022 June 03.

Published in final edited form as:

Sci Immunol. 2021 December 03; 6(66): eabi4493. doi:10.1126/sciimmunol.abi4493.

DDX17 is an essential mediator of sterile NLRC4 inflammasome activation by retrotransposon RNAs

Shao-bin Wang[1,2,*], **Siddharth Narendran**[1,2,3], **Shuichiro Hirahara**[1,2], **Akhil Varshney**[1,2], **Felipe Pereira**[1,2,4], **Ivana Apicella**[1,2], **Meenakshi Ambati**[1,2,5], **Vidya L. Ambati**[5], **Praveen Yerramothu**[1,2], **Kameshwari Ambati**[1,2], **Yosuke Nagasaka**[1,2], **Dionne Argyle**[1,2], **Peirong Huang**[1,2], **Kirstie L. Baker**[6], **Kenneth M. Marion**[6], **Kartik Gupta**[7], **Bo Liu**[7], **David R. Hinton**[8], **Scott W. Canna**[9], **Tamer Sallam**[10,11], **Srinivas R. Sadda**[6,12], **Nagaraj Kerur**[1,2,13,14], **Bradley D. Gelfand**[1,2,15], **Jayakrishna Ambati**[1,2,13,16,*]

[1]Center for Advanced Vision Science, University of Virginia School of Medicine, Charlottesville, VA, USA

[2]Department of Ophthalmology, University of Virginia School of Medicine, Charlottesville, VA, USA

[3]Aravind Eye Care System, Madurai, India

[4]Departamento de Oftalmologia e Ciências Visuais, Escola Paulista de Medicina, Universidade Federal de São Paulo, São Paulo 04023-062, Brazil

[5]Center for Digital Image Evaluation, Charlottesville, VA, USA

[6]Doheny Eye Institute, Los Angeles, Los Angeles, CA, USA

[7]Department of Surgery, University of Wisconsin-Madison, Madison, WI, USA

[8]Departments of Pathology and Ophthalmology, USC Roski Eye Institute, Keck School of Medicine of the University of Southern California, Los Angeles, CA, USA

[9]Pediatric Rheumatology & RK Mellon Institute for Pediatric Research, Children's Hospital of Pittsburgh of UPMC, Pittsburgh, PA, USA

[10]Division of Cardiology, Department of Medicine, David Geffen School of Medicine, University of California, Los Angeles, Los Angeles, CA, USA

[*]Correspondence: ja9qr@virginia.edu (J.A.); sw3ta@virginia.edu (S.W).

Author contributions: Conceptualization, S.W. and J.A.; Investigation, S.W., S.N., S.H., A.V., I.A., M.A., V.L.A., P.Y., K.A., F.P., Y.N. D.A., P.H., K.L.B., K.M.M., S.R.S; Writing, S.W., S.N., P.Y., K.A., N.K., B.D.G., and J.A with input from all authors. All authors had the opportunity to discuss the results and comment on the manuscript.

Competing interests:

J.A. is a co-founder of iVeena Holdings, iVeena Delivery Systems, and Inflammasome Therapeutics, and has been a consultant for Allergan, Boehringer-Ingelheim, Immunovant, Olix Pharmaceuticals, Retinal Solutions, and Saksin LifeSciences unrelated to this work. S.R.S. has been a consultant for 4DMT, Allergan, Apellis, Amgen, Centervue, Heidelberg, Iveric, Novartis, Optos, Oxurion, Regeneron, and Roche/Genentech, received speaker fees from Novartis, Nidek, Carl Zeiss Meditec, and Optos, and received research instruments from Carl Zeiss Meditec, Nidek, and Topcon, Centervue, Optos, Heidelberg unrelated to this work; J.A. and B.D.G. are co-founders of DiceRx. J.A., S.W., S.N., I.A., M.A., F.P., K.A., N.K., and B.D.G. are named as inventors on patent applications filed by their university.

Data and materials availability: The mass spectrometry proteomics data have been deposited to the ProteomeXchange Consortium via the PRIDE partner repository with the dataset identifier PXD016019 and 10.6019/PXD016019. All data needed to evaluate the conclusions in this paper are available in the paper or the Supplementary Materials.

[11]Molecular Biology Institute, Center for Health Sciences, David Geffen School of Medicine, University of California, Los Angeles, Los Angeles, CA, USA

[12]Department of Ophthalmology, David Geffen School of Medicine, University of California–Los Angeles, Los Angeles, CA, USA

[13]Department of Pathology, University of Virginia School of Medicine, Charlottesville, VA, USA

[14]Department of Neuroscience, University of Virginia School of Medicine, Charlottesville, VA, USA

[15]Department of Biomedical Engineering, University of Virginia School of Medicine, Charlottesville, VA, USA

[16]Department of Microbiology, Immunology, and Cancer Biology, University of Virginia School of Medicine, Charlottesville, VA, USA

Abstract

Detection of microbial products by multiprotein complexes known as inflammasomes is pivotal to host defense against pathogens. Nucleotide-binding domain leucine-rich repeat (NLR) CARD domain containing 4 (NLRC4) forms an inflammasome in response to bacterial products; this requires their detection by NLR family apoptosis inhibitory proteins (NAIPs), with which NLRC4 physically associates. However, the mechanisms underlying sterile NLRC4 inflammasome activation, which is implicated in chronic non-infectious diseases, remain unknown. Here, we report that endogenous short interspersed nuclear element (SINE) RNAs, which promote atrophic macular degeneration (AMD) and systemic lupus erythematosus (SLE), induce NLRC4 inflammasome activation independent of NAIPs. We identify DDX17, a DExD/H box RNA helicase, as the sensor of SINE RNAs that licenses assembly of an inflammasome comprising NLRC4, NLR pyrin domain-containing protein 3 (NLRP3), and apoptosis-associated speck-like protein containing CARD (ASC), and induces caspase-1 activation and cytokine release. Inhibiting DDX17-mediated NLRC4 inflammasome activation decreased interleukin-18 (IL-18) release in SLE patient peripheral blood mononuclear cells and prevented retinal degeneration in an animal model of AMD. Our findings uncover a previously unrecognized noncanonical NLRC4 inflammasome activated by endogenous retrotransposons and provide potential therapeutic targets for SINE RNA-driven diseases.

One Sentence Summary:

DDX17 senses retrotransposon RNA and activates a noncanonical NLRC4 inflammasome.

INTRODUCTION

Short interspersed nuclear element (SINE) elements are relatively short (< 700 nt) non-coding retrotransposons that account for more than 10% of the mass of mammalian genomes (1). Evolutionarily, SINEs originate from ancient pseudogenes of tRNAs, 7SL RNA, or 5S rRNA, and diverged into *Alu* elements in primates and B elements (B1 and B2) in rodents (2, 3). The genomic expansion of SINE elements requires two steps: RNA polymerase III-mediated transcription and L1-mediated reverse transcription and genomic integration (4). In somatic cells, almost all SINE elements are insertionally inactive; they become

transcriptionally active under conditions of cell stress such as virus infection, genome instability, or aging (5–7). Abnormal accumulation of SINE transcripts is increasingly recognized as a culprit in human diseases such as AMD (8), Alzheimer's disease (9, 10), multiple sclerosis (11), type 2 diabetes (12), and SLE (13). SINE RNAs induce inflammasome activation and degeneration of the retinal pigmented epithelium (RPE) in an NLRP3-dependent manner, but do not require a gamut of cytoplasmic RNA sensors including toll-like receptors, MDA5 and RIG-I (14), thereby leaving the question of the inflammasome-triggering sensor responsible for SINE RNA recognition unanswered.

The NBD-LRR (NLR)-containing proteins are a family of heterogeneous proteins that detect the presence of pathogen-associated molecular patterns (PAMPs) or endogenous danger-associated molecular patterns (DAMPs) (15). They typically comprise an N-terminal protein interaction domain, a central NBD and a C-terminal LRR domain (16). Of these inflammasomes, NLRP3 and NLRC4 inflammasomes are the best characterized and play important roles in the front-line of innate immunity to protect the host from various pathogenic infection (17, 18). Typically, the recognition of microbial stimuli by NLRP3 and NLRC4 is considered indirect, i.e., accessory sensor proteins are thought to be required for ligand recognition and licensing of NLRs activation. For example, assembly of the classical NLRC4 inflammasome requires NLR family, apoptosis inhibitory proteins (NAIPs), which sense the bacterial type III secretion apparatus and interact with NLRC4 in an oligomeric state and sequentially recruit ASC or procaspase-1, leading to its proteolytic cleavage and cytokine maturation (18, 19). Potassium efflux is a common step that is essential for NLRP3 inflammasome activation induced by various stimuli. In response to potassium efflux, the NIMA related kinase 7 (NEK7) acts as an essential partner that interacts with NLRP3 and licenses its activation (20, 21). In addition, crosstalk between NLRP3 and NLRC4 was revealed by studies in *E. coli*- and *S. typhimurium*-induced inflammation (22–24) and in sterile inflammation induced by lysophosphatidylcholine (LPC), hyperosmotic stress, or diacylglycerol (25–28). During *S. typhimurium* infection, NLRP3 and NLRC4 can be recruited to same macromolecular complex through ASC (29, 30). Interestingly, both NLRP3 and NLRC4 inflammasomes have been implicated independently in the pathogenesis of multiple sclerosis (26), a chronic inflammatory disease in which SINE RNA is upregulated (11), though the mechanisms regulating the assembly and activation of NLRC4 or NLRP3 inflammasome complexes remain to be elucidated in the context of sterile inflammation. Although the PAMPs-induced NLRC4 inflammasome has been extensively studied (31, 32), the mechanism of sterile NLRC4 inflammasome activation, which has been identified in many inflammatory disorders (33, 34), is relatively poorly understood. The roles of NAIPs in the sterile NLRC4 inflammasome are also largely unknown.

Here, we report that DDX17, a DExD/H box RNA family helicase without an established role in inflammasome activation, recognizes cytosolic SINE RNAs and licenses the assembly of an NLRC4 inflammasome complex that includes NLRP3, ASC, and caspase-1. This inflammasome platform facilitates the maturation of caspase-1, secretion of IL-1β and IL-18, and induction of cell death. Targeting this DDX17-mediated NLRC4 inflammasome inhibits RPE degeneration in a model of AMD and IL-18 release by SLE patient-derived

cells. These findings identify DDX17, NLRC4, and NLRP3 as potential drug targets in these and potentially other sterile inflammatory disorders.

RESULTS

SINE RNAs induce sterile NLRC4 inflammasome activation

To determine whether NLRC4 participates in SINE RNAs-induced inflammasome activation, we transfected primary mouse bone marrow-derived macrophages (BMDMs) isolated from wild-type or *Nlrc4*$^{-/-}$ mice with B2 or *Alu* RNA and monitored caspase-1 processing (p20), LDH release and IL-1β secretion. Notably, SINE RNA transfection in wild-type BMDMs induced caspase-1 p20 cleavage, LDH release and IL-1β secretion in a dose-dependent manner, which were greatly impaired in *Nlrc4*$^{-/-}$ BMDMs (Fig. 1, A and B, and fig. S1, A and B), suggesting that NLRC4 is essential for SINE RNA-induced inflammasome activation. Next, we sought to evaluate the activation of NLRC4 by measuring the phosphorylation of NLRC4 at serine 533 (S533), which contributes to PAMP-induced NLRC4 inflammasome activation (35–37). SINE RNA transfection induced NLRC4 S533 phosphorylation and caspase-1 cleavage in wild-type mouse BMDMs (Fig. 1C and fig. S1C).

Oligomerization of NLRC4 is important in initiating assembly and subsequent activation of the NLRC4 inflammasome (38). Using native polyacrylamide gel electrophoresis, we observed the formation of large oligomeric NLRC4 complexes induced by *Alu* RNA (Fig. 1D). ASC, which undergoes condensation into a massive insoluble oligomer known as the apoptotic speck during inflammasome activation (32, 38), enhances NLRC4-induced caspase-1 activation (24). We observed formation of ASC and NLRC4 double-positive specks as well as ASC oligomers in SINE RNA-transfected mouse BMDMs (Fig. 1, E and F and fig. S1, D to F). In the PAMP-induced NLRC4 inflammasome, NLRC4 can interact directly with caspase-1 in the absence of ASC (39). To evaluate the roles of NLRC4 and ASC in SINE-RNA inflammasome activation, we studied the requirement of ASC (encoded by *Pycard*) in bacterial flagellin- and SINE RNAs-induced NLRC4 inflammasome. Consistent with previous studies, NLRC4-dependent caspase-1 activation and IL-1β secretion induced by cytosolic flagellin (*S. typhimurium*) were partially inhibited in BMDMs isolated from *Pycard*$^{-/-}$ mice (Fig. 1G and fig. S1, G and H), suggesting an alternative ASC-independent signaling in canonical NLRC4 inflammasome formation. In contrast, low-grade caspase-1 activation and IL-1β secretion induced by SINE RNAs were largely inhibited in *Pycard*$^{-/-}$ and *Nlrc4*$^{-/-}$ BMDMs.

A hallmark of bacterial induced NLRC4 inflammasome is pyroptosis, which is driven in part by caspase-1-mediated cleavage of the pore-forming protein gasdermin D (GSDMD, encoded by *Gsdmd*) (40, 41). Interestingly, we previously demonstrated that although GSDMD is required for *Alu* RNA-induced RPE degeneration, *Alu* RNA does not induce the canonical cleavage of GSDMD that occurs in response to intracellular LPS and drives pyroptosis (42). We also showed that a mutant GSDMD incapable of canonical cleavage supported *Alu* RNA-induced cell death, suggesting a non-pyroptotic role for GSDMD in this context. This non-canonical role of GSDMD in *Alu* RNA-mediated RPE degeneration is consistent with our observation that *Alu* RNA promotes cell death primarily via apoptosis

and not pyroptosis (42). Here, we studied the role of GSDMD in the setting of B2 RNA and found that, whereas cytosolic LPS and flagellin triggered canonical GSDMD p30 cleavage, B2 RNA did not do so (fig. S1I). However, B2 RNA-induced IL-1β secretion was largely reduced in *Gsdmd*$^{-/-}$ BMDMs (fig. S1J), implicating a potential nonlytic role of GSDMD in the SINE RNA-induced sterile NLRC4 inflammasome activation (43), consistent with our earlier observations on the role of GSDMD in the setting of *Alu* RNA (42). Together, these results suggest that SINE RNAs induce an ASC-dependent sterile NLRC4 inflammasome activation. The LDH release we observed is compatible with our earlier finding that cells transfected with *Alu* RNA eventually display characteristics of late apoptosis or secondary necrosis (42). Importantly, LDH release was also NLRC4-dependent.

Sterile NLRC4 inflammasome requires PKCδ but not NAIPs

The above results suggested that phosphorylation of NLRC4 at serine 533 (S533) occurs in response to SINE RNA stimulation. To study the role of NLRC4 phosphorylation in SINE RNA-induced inflammasome activation, we tested inflammasome activation induced by SINE RNAs in BMDMs isolated from homozygous non-phosphorylatable NLRC4 (S533A) mutant mice (44). We found that SINE RNA-induced caspase-1 cleavage and IL-1β secretion were largely impaired in S533A mutant BMDMs, despite having intact NLRC4 expression (Fig. 2, A and B, and fig. S2A). To identify the mechanisms governing NLRC4 phosphorylation, we studied two kinases reported to phosphorylate NLRC4 at S533: protein kinase C delta (PKCδ, encoded by *PRKCD*) (35) and leucine rich repeat-containing kinase-2 (LRRK2) (37). We treated wild-type BMDMs with GSK2578215A, an inhibitor of LRRK2, or with rottlerin, an inhibitor of PKCδ. Rottlerin, but not GSK2578215A, inhibited *Alu* RNA-induced phosphorylation of NLRC4 and caspase-1 activation in BMDMs in a dose-dependent manner (fig. S2B), providing pharmacological evidence that PKCδ might be involved in SINE RNA-induced NLRC4 phosphorylation. Next, we investigated the requirement of PKCδ in BMDMs isolated from *Prkcd*$^{+/+}$, *Prkcd*$^{+/-}$, and *Prkcd*$^{-/-}$ mice. We found a gene dosage-dependent reduction in *Alu* RNA-induced NLRC4 phosphorylation and IL-1β release in *Prkcd* mutant BMDMs (Fig. 2, C and D and fig. S2C). In addition, depletion of the PKCδ protein via *PRKCD* siRNA transfection into human monocytic THP-1 cells impaired caspase-1 cleavage and release of IL-1β and IL-18 (fig. S2, D to F). Collectively, these pharmacological and genetic data demonstrate that PKCδ-dependent NLRC4 phosphorylation is important for sterile NLRC4 inflammasome activation.

NAIPs are essential for NLRC4 inflammasome activation induced by bacterial PAMPs (45, 46). Mouse NAIP5 and NAIP2 form complexes with NLRC4 upon binding flagellin or T3SS components of *Salmonella* species, respectively (19). In humans, the sole full-length NAIP senses both flagellin and T3SS components (47, 48). Thus, we sought to determine whether NAIPs are required for SINE RNA-induced NLRC4 inflammasome activation. In accord with previous reports (19, 49), we found that cytosolic flagellin-induced caspase-1 cleavage and IL-1β release, which are mediated by NAIP5 and NLRC4, were largely impaired in BMDMs isolated from mice deficient for all NAIP paralogs (*Naip1-6*$^{\Delta/\Delta}$) (Fig. 2, E and F). Surprisingly, *Alu* RNA-induced caspase-1 activation, which also is mediated by NLRC4 (Fig. 1C and fig. S1A), was unimpaired in *Naip1-6*$^{\Delta/\Delta}$ BMDMs (Fig. 2G). *Alu* RNA and B2 RNA also induced comparable release of IL-1β in both wild-type and *Naip1-6*$^{\Delta/\Delta}$

BMDMs (Fig. 2H). In addition, *Alu* RNA-induced IL-1β release in THP-1 cells was reduced by *NLRC4* siRNA but not *NAIP* siRNA (fig. S2G). Together, these findings demonstrate that NAIPs, the conventional PAMP-sensing proteins, are dispensable for sterile NLRC4 inflammasome activation induced by SINE RNAs, identifying a previously unidentified NAIP-independent mechanism of NLRC4 activation.

DDX17 recognizes SINE RNAs for sterile inflammasome activation

To date, the cytosolic sensors of SINE RNAs necessary for noncanonical NLRC4 inflammasome activation are unknown. To identify proteins that interact with SINE RNAs, we transfected human THP-1 monocytic cells with biotinylated *Alu* RNA or free biotin, and purified *Alu* RNA-associated complexes using streptavidin affinity pulldown. Using liquid chromatography–mass spectrometry (LC-MS), we identified twelve proteins significantly enriched in biotinylated *Alu* RNA-treated samples, of which five – 2'-5'-oligoadenylate synthetase 2 (OAS2), eukaryotic translation initiation factor 2 alpha kinase 2 (EIF2AK2 or PRKR), DExH-Box Helicase 58 (DHX58), DEAD-Box Helicase 5 (DDX5) and DEAD-Box Helicase 17 (DDX17) – were known RNA binding proteins (fig. S3A). To determine which of these five proteins were required for SINE RNA-induced inflammasome activation, we targeted each of these five candidates individually using siRNAs; only *DDX17* siRNA reduced IL-1β release in *Alu* RNA-transfected THP-1 cells (fig. S3, B and C), suggesting that DDX17 could be the sensor of SINE RNAs that licenses inflammasome activation. Of note, EIF2AK2 was previously reported to bind *Alu* RNA and repress inflammasome activity by inhibiting protein translation of inflammasome constituents (50, 51). Consistent with those observations, we found that EIF2AK2 knockdown increased IL-1β release in THP-1 cells (fig. S3B).

To confirm the interaction between DDX17 and SINE RNAs, we performed competitive binding assays in human embryonic kidney (HEK293T) cells with biotinylated *Alu* RNA or biotinylated B2 RNA. Following exogenous expression of Myc-tagged DDX17, we detected specific interactions with both biotinylated *Alu* RNA and biotinylated B2 RNA that were competitively inhibited by unlabeled SINE RNAs, but not by 7SL RNA, a structurally related non-SINE RNA (Fig. 3A and fig. S3D). We next sought to visualize the interaction of DDX17 and SINE RNAs *in situ* via immunofluorescence. In THP-1 cells, *Alu* RNA transfection induced translocation of DDX17 from the nucleus to the cytoplasm (Fig. 3B), akin to the response in U2OS epithelial cells following viral infection (52), and increased formation of cytosolic puncta wherein DDX17 was colocalized with *Alu* RNA in human RPE cells (fig. S4A).

To further test whether DDX17 is required for SINE RNA-induced inflammasome activation, we generated tetracycline-inducible (iDDX17 shRNA) DDX17 shRNA-expressing THP-1 cells (fig. S4B). In these cells, depletion of DDX17 protein induced by doxycycline (Dox) treatment blocked SINE RNA-induced caspase-1 activation and IL-1β release (fig. S4C). Inflammasome regulation can differ between human and mouse systems (53). Therefore, to test whether the role of DDX17 in inflammasome regulation is conserved in mouse cells, we measured caspase-1 cleavage and IL-1β release in immortalized *Ddx17*$^{+/+}$ and *Ddx17*$^{-/-}$ bone marrow-derived macrophages (iBMDMs). *Alu* RNA induced

caspase-1 activation and IL-1β release in *Ddx17*$^{+/+}$ but not *Ddx17*$^{-/-}$ iBMDMs (Fig. 3, C and D). B2 RNA-induced caspase-1 activation was abrogated in *Ddx17*$^{-/-}$ iBMDMs; this was rescued by lentivirus-mediated constitutive overexpression of DDX17 (fig. S4D). These data suggest a conserved role of DDX17 in regulating inflammasome activity in both mouse and human cells.

Since DDX5 shares high sequence identity and marked functional similarity with DDX17, we sought to distinguish the roles of these close paralogues. We studied caspase-1 cleavage and IL-1β release, hallmarks of inflammasome activation in siRNA-transfected THP-1 cells. An siRNA targeting a sequence common to DDX5 and DDX17 blocked *Alu* RNA-induced caspase-1 activation and IL-1β levels in either the supernatant or cell lysates of THP-1 cells (Fig. 3, E and F). Next, we tested knockdown of these genes individually. Whereas DDX17 siRNA inhibited *Alu* RNA-induced inflammasome activation, DDX5 siRNA did not do so (Fig. 3, E and F). DDX17 is also involved in nuclear miRNA processing as components of the DROSHA microprocessor complex. However, *Alu* RNA induced comparable levels of IL-1β release in *DROSHA* siRNA- and control siRNA-treated THP-1 cells (fig. S4, E and F). Together, these observations suggest that DDX17, but not DDX5, acts as a cytoplasmic SINE RNAs sensor that mediates inflammasome activation independent of its nuclear microprocessor-associated function.

NLRC4 cooperates with NLRP3 in the SINE RNA-induced sterile inflammasome

Previously, we demonstrated that NLRP3 is required for *Alu* RNA-induced inflammasome activation (14). Recent studies suggest that NLRP3 and ASC can be recruited by NLRC4 during canonical NLRC4 inflammasome activation by bacterial infection (29, 30). We therefore investigated the role of NLRP3 in SINE RNA-induced NLRC4 inflammasome activation. Firstly, caspase-1 cleavage and IL-1β release induced by *Alu* RNA or B2 RNA were inhibited in *Nlrp3*$^{-/-}$ BMDMs (Fig. 4, A and B). Likewise, ASC oligomerization was reduced in *Nlrp3*$^{-/-}$ BMDMs (Fig. 4C). In addition, inhibitors targeting NLRP3 (MCC950) or PKC-δ (Rottlerin) significantly dampened B2 RNA-induced IL-1β release (fig. S5A). To test whether this sterile inflammasome is involved in the setting of endogenous SINE RNA accumulation, we used a model of DICER1 deficiency, which induces SINE RNA accumulation (fig. S5B) and inflammasome activation (14, 54, 55). We found that Dicer1 knockdown-induced caspase-1 cleavage was inhibited in *Nlrp3*$^{-/-}$ and *Nlrc4*$^{-/-}$ BMDMs when compared to wild-type BMDMs (fig. S5C). These findings suggest that both endogenous and exogenous SINE RNAs induce sterile inflammasome activation in a manner requiring NLRP3 and NLRC4.

Redundant roles of NLRP3 and NLRC4 have been reported in both PAMP- and DAMP-induced inflammasomes (23, 24). To explore the redundancy of NLRP3 and NLRC4 in the SINE RNAs-induced inflammasome, we assessed B2 RNA-induced inflammasome activity in BMDMs isolated from wild-type (WT), *Nlrp3*$^{-/-}$, *Nlrc4*$^{-/-}$, and *Nlrp3*$^{-/-}$ *Nlrc4*$^{-/-}$ double knockout mice. We observed that B2 RNA-induced caspase-1 cleavage and IL-1β release were similarly reduced in *Nlrp3*$^{-/-}$, *Nlrc4*$^{-/-}$ and *Nlrp3*$^{-/-}$ *Nlrc4*$^{-/-}$ BMDMs (Fig. 4D and fig. S5D), suggesting non-redundant, and perhaps mutually dependent, roles of NLRP3 and NLRC4 in the SINE RNA-induced inflammasome.

Intriguingly, we observed assembly of NLRC4-NLRP3 complexes after B2 RNA transfection by co-immunoprecipitation assay (fig. S5E). This interaction prompted us to dissect the order of recruitment of the various proteins involved in this sterile inflammasome. We observed that *Alu* RNA induced interaction of NLRP3 and ASC (encoded by *Pycard*) in wild-type but not *Nlrc4*$^{-/-}$ BMDMs (Fig. 4E). In contrast, SINE RNA induced NLRC4 phosphorylation in wild-type as well as *Nlrp3*$^{-/-}$ and *Pycard*$^{-/-}$ BMDMs (fig. S5F). Together, these results suggest that NLRC4 phosphorylation precedes ASC recruitment in the SINE RNA-induced sterile inflammasome. Consistent with this model, we observed reduced *Alu* RNA-induced ASC oligomerization in *Nlrc4*$^{-/-}$ BMDMs (fig. S1D).

DDX17 licenses sterile NLRC4 inflammasome assembly

Since DDX17 is required for inflammasome activation, we next investigated the role of DDX17-SINE RNA interaction in NLRC4-NLRP3-ASC complex assembly. We transfected THP-1 cells with *Alu* RNA and purified the DDX17-associated complexes for liquid chromatography–mass spectrometry (LC–MS) analysis. We found that *Alu* RNA transfection enhanced the formation of DDX17-NLRC4 and DDX17-NLRP3 complexes (Fig. 4F and table S1). SINE RNA-induced interaction between DDX17 and NLRC4 in wild-type BMDMs was confirmed by co-immunoprecipitation and immunofluorescence assays (fig. S5, G to I). Interestingly, SINE RNA-induced DDX17-NLRC4 and DDX17-NLRP3 complexes were observed in wild-type as well as *Pycard*$^{-/-}$ BMDMs (fig. S5I). Notably, SINE RNAs-induced NLRC4-NLRP3 interaction was diminished in *Ddx17*$^{-/-}$ BMDMs (Fig. 4G), and ASC oligomerization induced by SINE RNAs was reduced by DDX17 siRNA (Fig. 4H). Collectively, these data are compatible with a model that DDX17 is essential for NLRC4-NLRP3-ASC inflammasome assembly.

To determine the regions within NLRC4 that associate with DDX17, we expressed Flag-tagged full-length NLRC4 or various GFP-tagged domains of NLRC4 in HEK293T cells. DDX17 interacted with full-length NLRC4 and with the NACHT domain of NLRC4, but not with its LRR or CARD domains when co-expressed in HEK293T cells (fig. S6A). Conversely, NLRC4 interacted with full-length DDX17 and the helicase domain of DDX17, but not with its N-terminal or C-terminal domains (fig. S6B).

Since DDX17 is essential for NLRC4-NLRP3 inflammasome assembly, we sought to test whether DDX17 is required in other classical models of inflammasome activation. We examined activation of the NLRP3, caspase-11, and NLRC4 inflammasomes using their respective canonical agonists in THP-1 cells. Whereas DDX17 knockdown blunted caspase-1 activation due to SINE RNA, it did not affect caspase-1 activation when treated with LPS and ATP (triggers of the canonical NLRP3 inflammasome), intracellular LPS (caspase-11 inflammasome activator), or flagellin (trigger of canonical NLRC4 inflammasome) (fig. S7A). Similarly, DDX17 knockdown inhibited IL-1β and IL-18 release in response to SINE RNA but not to other inflammasome-activating stimuli (fig. S7, B and C). These results identify a specific role for DDX17 in mediating inflammasome activation triggered by SINE RNA but not microbial PAMPs.

DDX17-mediated sterile NLRC4 inflammasome activation *in vivo*

Alu RNA accumulation has been reported in several human diseases including AMD and SLE (8, 13). To gain insights into the role of the DDX17-NLRC4 inflammasome in a human disease context, we studied primary peripheral blood mononuclear cells (PBMCs) isolated from patients with active SLE (table S2), in which increased *Alu* RNA levels have been reported (13). Consistent with those earlier findings, we observed, via northern blotting, a robust increase in the abundance of ~300-nt long full-length *Alu* RNA in SLE PBMCs compared to PBMCs from healthy controls (Fig. 5A). The abundance of DDX17 mRNA and protein, but not of NLRC4, was increased in SLE PBMCs (Fig. 5, B to D). In addition, increased levels of phosphorylated PKCδ (Tyr311), which accompany NLRC4 activation (27), and of cleaved caspase-1 (p20) were observed in SLE PBMCs (Fig. 5, C and E), supportive of DDX17-NLRC4 inflammasome activation in SLE.

Next, we studied assembly of the DDX17-NLRC4 inflammasome in the setting of SLE. First, we performed fluorescence *in situ* hybridization (FISH) and proximity ligation assay (PLA) to detect the existence of *Alu* RNA-DDX17 complexes. In SLE PBMCs, we observed cytosolic DDX17 puncta colocalized with *Alu* RNA, which was visualized by digoxigenin (DIG)-labeled RNA probes (Fig. 5, F and G and fig. S8A). PLA also provided evidence of *Alu* RNA-DDX17 proximity in the cytoplasm of SLE PBMCs (fig. S8, B and C). Second, the assembly of NLRC4-ASC complexes was visualized by immunofluorescence. We found that ASC and NLRC4 double-positive specks were increased in SLE PBMCs compared to healthy control cells (fig. S8, D and E). Together these findings suggest that *Alu* RNA in SLE PBMCs interacts with cytosolic DDX17 and induces assembly of a sterile NLRC4 inflammasome.

Elevated serum levels of interleukin-18 (IL-18) and IL-1β are hallmarks of SLE, and IL-18 inhibition alleviates disease pathology in models of SLE (56). However, serum IL-1β was undetectable in the majority of SLE samples (57). In our SLE PBMC cultures, only IL-18 was detectable with LPS priming, and inhibition of NLRC4 phosphorylation by a PKCδ inhibitor or treatment with siRNAs targeting DDX17, NLRP3 or NLRC4 reduced IL-18 levels in SLE cells (Fig. 5H and fig. S8, F to K), suggesting the existence of a functional DDX17-NLRC4/NLRP3 inflammasome in SLE PBMCs.

SINE RNAs induce RPE degeneration in geographic atrophy, a late stage of AMD that has no approved treatment (8). NLRP3 is required for SINE RNA-induced RPE degeneration (14), as well as for sterile NLRC4 inflammasome activation in BMDMs, as shown above. To elucidate the hierarchy of NLRC4 and NLRP3 in the RPE, we evaluated interactions between NLRC4 and NLRP3, NLRP3 and ASC, and NLRC4 and ASC in primary human RPE cells using PLA. *Alu* RNA treatment induced a striking increase in the number of NLRC4-NLRP3 puncta and NLRP3-ASC puncta, but a less robust increase in NLRC4-ASC puncta (Fig. 6, A and B), suggesting that NLRP3 might bridge NLRC4-NLRP3-ASC complexes induced by SINE RNAs in the RPE. In addition, *NLRC4* siRNA, but not *NAIP* siRNA, reduced ASC oligomerization in *Alu* RNA-treated human RPE cells (Fig. 6C).

Next, we investigated NLRC4 inflammasome activation in a mouse model of RPE degeneration. Subretinal injection of SINE RNA induced RPE degeneration in wild-type

but not *Nlrc4*$^{-/-}$ mice (Fig. 6D). Furthermore, knockdown of *Ddx17* blocked SINE RNA-induced RPE degeneration in wild-type mice (Fig. 6, E and F). In contrast, *Naip1-6*$^{\Delta/\Delta}$ mice were not protected (fig. S9A). Consistent with our observation that PKCδ is required for SINE RNAs-induced NLRC4 inflammasome, we found that *Nlrc4*$^{S533A/S533A}$ and *Prkcd*$^{-/-}$ mice were protected against *Alu* RNA-induced RPE degeneration (fig. S9, B and C). These data provide *in vivo* evidence that DDX17 and NLRC4, but not NAIPs, are critical for SINE RNA-induced RPE degeneration.

DISCUSSION

Our studies reveal endogenous SINE RNAs as previously undescribed inducers of NLRC4 inflammasome activation and also identify the existence of a NAIP-independent, DDX17-dependent noncanonical NLRC4 inflammasome (fig. S10). In accord with prior studies on NLRC4 inflammasomes in sterile inflammation (27, 33), this noncanonical NLRC4 inflammasome was characterized by low-grade caspase-1 activation and cytokine release compared to microbial PAMP-induced NLRC4 inflammasome activation. Interestingly, SINE RNA-induced NLRC4 inflammasome activation does not requires NAIPs, the conventional sensors essential for bacterial PAMP-induced NLRC4 inflammasome activation. Instead, we demonstrate its dependence on the RNA helicase, DDX17, suggesting the existence of several potentially stimulus-specific sensors capable of inducing diverse modes of NLRC4 activation. Indeed, previous reports have indirectly inferred the possibility of NAIP-independent NLRC4 inflammasome activation in response to both sterile stimuli such as diacylglycerol (DAG) and LPC, and microbial stimuli such as *Candida albicans* and *Anaplasma phagocytophilum* (58, 59). We now provide direct genetic evidence of a sterile NAIP-independent NLRC4 inflammasome that is activated by retrotransposon RNAs.

It is worth noting that the requirement of PKCδ-mediated NLRC4 phosphorylation we identified in SINE RNAs-induced inflammasome activation is not incompatible with the recent finding that PKCδ and NLRC4 phosphorylation are dispensable for PAMP-induced NLRC4 inflammasome (44, 60), as these studies reported that NLRC4 phosphorylation was indeed important for low-level ligand stimulation of NLRC4, which may actually reflect the NLRC4 inflammasome response to endogenous, non-infectious stimuli (44). These observations also shed light on the potential differences in the mechanisms regulating NLRC4 inflammasome activation in non-infectious settings compared to bacterial infections. These differences may arise from the variation in the kinetics, magnitude and characteristics of the inflammatory response to “danger” (PAMPs/infectious) versus “damage” (DAMPs/sterile) stimuli, as the latter is a critical component of the immune system in maintaining tissue homeostasis. Such differences in responses have been previously observed in variable NLRP3 inflammasome responses (61). Although our data suggest a non-redundant role of NLRC4 and NLRP3 in the SINE RNA-induced inflammasome, it is conceivable that the lower magnitude of sterile NLRC4 inflammasome activation induced by SINE RNA could mask the redundancy of NLRC4 and NLRP3 present in other contexts. Indeed, NLRC4-independent caspase-1 activation and cytokine release were observed with high dose SINE RNA stimulation. Thus, the precise mechanism of how NLRC4 collaborates with NLRP3 requires further investigation.

In this study, we provide several lines of evidence to support DDX17 as a previously unidentified inflammasome sensor for SINE RNAs. Recently, DExD/H box RNA helicases have been implicated in the activation of various inflammasomes: DHX33 or DDX19A for viral RNA-induced NLRP3 inflammasome (62, 63); DDX3X for stress granule-mediated NLRP3 inflammasome (64); DHX9 for rotavirus-induced NLRP9b inflammasome (65); and DHX15 for NLRP6-mediated antiviral immunity (66). However, DDX17 has not previously been implicated in inflammasome activation. Instead, DDX17 is best known for its roles in normal miRNA processing and regulating RNA splicing and export along with its close homolog DDX5 as well as in the context of antiviral defense (52).

Unlike many other inflammasome sensors that are generally controlled by separate priming and activation steps, DDX17 does not undergo translational priming in response to SINE RNAs stimulation. Instead, DDX17 translocates from the nucleus to the cytoplasm and forms cytoplasmic puncta containing SINE RNAs and NLRC4. We speculate this translocation allows DDX17 to access and orchestrate other inflammasome adaptors such as NLRC4. However, the mechanism of how SINE RNA induces DDX17 translocation is unknown. In cancer cells, DDX17 undergoes nucleocytoplasmic shuttling during drug resistance through an exportin/importin-dependent pathway (67). How DDX17 specifically binds SINE RNAs also remains to be elucidated. To date, there are two reported characteristics defining the specificity of DDX17 in recognizing RNA molecules: the secondary structure of the RNA stem-loop and the unique RCAYCH motif of an RNA sequence (52, 68). Of note, SINE RNAs contain both a stem-loop structure and a RCAYCH motif, which may underlie recognition by DDX17 (69).

DDX17 recognizes a spectrum of RNA species, including viral RNA, host miRNA or lncRNA. Whether the homeostatic dysregulation of these RNAs can trigger the activation of sterile NLRC4 inflammasome requires further investigation. In summary, we identify DDX17 as the cytoplasmic sensor of SINE RNAs and that it is required for sterile NLRC4 inflammasome activation in this context. Our observation that DDX17 and NLRC4 are required for inflammasome activation and IL-18 release in SLE and also for RPE degeneration in a model of AMD suggests that DDX17 and NLRC4 could represent attractive targets for diseases in which SINE RNA dysregulation has been implicated.

MATERIALS AND METHODS

Study design

The goal of this study was to determine the intracellular sensor that recognizes SINE RNA and licenses downstream inflammasome activation. Initially, we profiled SINE RNA interactors by pulldown and mass spectrometry analysis, and we identified DDX17 as the sensor that is required for SINE RNA-induced inflammasome activation. We explored the composition of DDX17-containing complexes by co-immunoprecipitation and mass spectrometry and found that they contain NLRP3 and NLRC4 inflammasome components. Validation of NLRP3 and NLRC4 inflammasome activation was performed by functional assessment of inflammasome activity by using *in vitro* transduction experiments in primary BMDM cells isolated from various KO mice. To better understand the *in vivo* roles of this DDX17-dependent inflammasome, we tested the requirement of DDX17-NLRC4/NLRP3

signaling in two SINE RNA-associated models: endogenous *Alu* RNA-related SLE and SINE RNA-induced RPE degeneration. For *in vitro* studies, as least three independent experiments were performed. For *in vivo* studies, all mice were housed in the same room, and were randomly assigned for experiments. The RPE degeneration graders were blind to mouse genotype and treatment identity. The sample size is specified in each figure legend.

Mice

Wild-type (WT) C57BL/6J mice were purchased from The Jackson Laboratory. *Nlrc4*$^{-/-}$ (70), *Nlrc4*$^{S533A/S533A}$ (44), *Nlrp3*$^{-/-}$ (71), *Pycard* (also known as *Asc*)$^{-/-}$ (71), and *Naip1-6*$^{\Delta/\Delta}$ (19)mice have been previously described. *Prkcd*$^{+/-}$ (72) mice were a generous gift from Dr. Bo Liu (University of Wisconsin), and used to generate *Prkcd*$^{+/+}$ and *Prkcd*$^{-/-}$ mice. *Nlrp3*$^{-/-}$ mice were interbred with *Nlrc4*$^{-/-}$ mice to generate *Nlrp3*$^{-/-}$ *Nlrc4*$^{-/-}$ “double knockout” mice. All mice were bred and housed in a pathogen-free laminar flow facility at the University of Virginia. For all procedures, anesthesia was achieved by intraperitoneal injection of 100 mg/kg ketamine hydrochloride (Ft. Dodge Animal Health) and 10 mg/kg xylazine (Phoenix Scientific), and pupils were dilated with topical 1% tropicamide and 2.5% phenylephrine hydrochloride (Alcon Laboratories). Mice were treated in accordance with the guidelines of the University of Virginia’s Institutional Animal Care & Use Committee and the Association for Research in Vision and Ophthalmology. Both male and female mice between 6 and 10 weeks of age were used.

Cell culture

Primary WT or mutant mouse bone marrow derived macrophages (BMDMs) were isolated as previously described (73). DDX17-deficient and wildtype immortalized bone marrow-derived macrophages (iBMDMs) were a generous gift from T.I. Sallam (UCLA) (74). BMDMs or iBMDMs were cultured in IMDM (Gibco) basal medium with 10% fetal bovine serum (FBS) and 30% L929 supernatants, non-essential amino acids, sodium pyruvate, 2-mercaptoethanol and antibiotics. THP-1 cells and primary PBMCs (Precision Medicine Group, US) were cultured in RPMI-1640 medium with 10% FBS and antibiotics. Human RPE cells were isolated as previously described (75), and cultured in DMEM with 10% FBS and antibiotics. All cells were maintained at 37 °C in a 5% CO_2 environment.

In vitro synthesis of SINE RNAs

Alu, B2, B1, and 7SL RNAs, and biotinylated RNAs were synthesized from a linearized plasmid containing a consensus SINE sequences with an adjacent 5′ T7 promoter, subjected to AmpliScribe T7 Flash Transcription kit according to the manufacturer’s instructions. DNase-treated RNAs were purified using MEGAclear (Ambion) and integrity was confirmed by agarose gel electrophoresis.

Cell transfection and stimulation

Flagellin (3 μg/ml) and LPS (5 μg/ml) transfections were performed according to the manufacturer’s instructions (DOTAP Liposomal Transfection Reagent). In addition to LPS priming, pre-seeded or pre-treated THP-1 cells or BMDMs were stimulated with ATP (5 mM) for 30 min. For ELISA measurements of IL-18 and IL-1β, BMDM cells or

THP-1 cells were primed by LPS (125 ng/ml) for 4 h, and then washed with serum-free medium for subsequent treatment. HEK293 cells were transfected using Lipofectamine 3000 (Invitrogen) was used. siRNA (25 nM for BMDMs; 100 nM for THP-1 cells) transfection was performed using Viromer® BLUE (VB-01LB-00, Lipocalyx) according to the manufacturer's instructions. Serum free media was collected for ELISA or TCA precipitation. Cell pellets were collected for RNA extraction or immunoblotting. "Mock" denotes the use of transfection reagents alone in all experiments.

Immunoprecipitation and streptavidin affinity pull down

Prior to lysis, pre-stimulated cells were detached with a cell scraper and transferred into a microcentrifuge tube on ice. After centrifugation for 7 min at 400 g at 4 °C, the cell pellet was washed twice with ice-cold PBS (without Ca^{2+} and Mg^{2+}; pH 7.1). The washed cell pellet was resuspended in lysis buffer (50 mM Tris, 2 mM EDTA, 150 mM NaCl, 0.5% Nonidet P-40) complemented with protease inhibitors. After centrifugation for 10 min at 12,000 rpm at 4 °C, the supernatant was washed using protein A/G magnetic beads (Invitrogen) to prevent any non-specific binding. The samples were incubated with primary antibodies and were pulled down using protein A/G beads at 4 °C overnight.

For streptavidin bead pull down, THP-1 cells were treated with biotin-conjugated SINE RNAs or competitive molecules. After centrifugation for 10 min at 400g at 4 °C, the cell pellet was washed twice with ice-cold PBS and subjected to cross-linking with UV irradiation (150 mJ/cm^2, Stratalinker). Cells were harvested and lysed with ice-cold lysis buffer (150 mM NaCl, 25 mM Tris pH 7.4, 5 mM EDTA, 0.5 mM DTT, 0.5% NP40) and then subjected to streptavidin binding with Dynabeads® M-280 streptavidin at 4 °C overnight. Purified RNA-protein or protein-protein complexes were eluted with elution buffer (100 mM glycine-HCl, pH 2.8 for protein-protein and 50 mM Tris HCl pH 7.4 with 25 nM biotin for RNA-protein) and analyzed by immunoblotting or LC-MS/MS.

Mass spectrometry

LC-MS/MS experiments were performed at the Biomolecular Analysis Facility of UVA using a Thermo Electron Q Exactive HF-X mass spectrometer system with an Easy Spray ion source connected to a Thermo 75 μm × 15 cm C18 Easy Spray column (through pre-column). Briefly, purified RNA-protein or protein-protein complexes were boiled with SDS sample buffer and concentrated with 7.5% Mini-PROTEAN® TGX™ Precast Protein Gels (4561023, Bio-Rad). The gel pieces were subsequently washed with 50% methanol. Samples were alkylated and then digested overnight at 37 °C. The digest was analyzed using the rapid switching capability of the instrument acquiring a full scan mass spectrum to determine peptide molecular weights followed by product ion spectra (10 HCD) to determine amino acid sequence in sequential scans. These data were analyzed using the Sequest search algorithm against Uniprot and SwissProt.

Lentivirus production and transduction

The lentivirus plasmid coding human DDX17 protein, pLenti-GIII-CMV-DDX17-GFP-2A-Puro, was constructed by Abmgood (LV134653), pLenti-CMV-GFP-Zeo was obtained from Addgene (#17449). Lentiviral particles were produced with packaging mix (Abm, LV003)

and Lenti-X 293T cells as per the manufacturer's instructions. Lentiviruses were collected 48h and 96h post transfection, purified and concentrated with Amicon Ultra centrifugal filters (mwco 100 kDa) and stored at −80 °C. *Ddx17*$^{-/-}$ iBMDM cells were transduced with lentivirus particles mixed with 3 μg/ml polybrene, and positive cell clones were selected by GFP signal.

Enzyme-linked immunosorbent assay (ELISA) and LDH release assay

Secreted human and mouse IL-1β and IL18 in the medium were detected by ELISA (Human IL-1β/IL-1F2 DuoSet, R&D Systems, DY201; Mouse IL-1β/IL-1F2 DuoSet, R&D Systems, DY401, Human Total IL-18/IL-1F4) according to the manufacturer's instructions. LDH release was measured by using CytoTox 96 Non-Radioactive Cytotoxicity Assay (Promega) by following the manufacturer's instructions.

ASC oligomerization assay

BMDMs, THP-1 or human RPE cells were seeded at 1×10^6/ml in 6-well plates. 24 h later, cells were washed twice with ice-cold PBS prior to their collection. The washed cells were resuspended in pre-chilled lysis buffer (NaCl 150 mM, HEPES 50 mM, 1% NP40) for 30 min. Lysates were centrifuged for 10 min at 1000g at 4 °C, supernatants were transferred into new tubes (as soluble fractions). The pellets were washed twice in 1 ml ice-cold PBS and resuspended in 500 μl PBS, 2 mM disuccinimydyl suberate and incubated for 30 min at room temperature with rotation. The cross-linked pellets were spin down and then boiled with NuPAGE LDS Sample Buffer (Thermo Fisher Scientific) and analyzed by immunoblotting.

TCA/Acetone Precipitation

Stimulated BMDMs or THP-1 cells were detached with a cell scraper and transferred into a microcentrifuge tube on ice. After centrifugation for 10 min at 12,000 rpm at 4 °C, 1 ml of serum free medium was transferred into fresh tubes. 15 μl of 10% sodium deoxycholate was added to the supernatants, vortexed and keep on ice. 100 μl Trichloroacetic acid was subsequently added and the tubes were kept on ice overnight. After centrifugation for 30 min at 12,000 rpm at 4 °C pellet was washed with 500 μl ice-cold acetone. The pellet was dried and boiled with LDS Sample Buffer and Sample Reducing Agent. The precipitated protein was analyzed by immunoblotting.

Immunofluorescence staining and PLA assay

Stimulated BMDMs or human RPE cells were plated in an 8-well chamber slide (154941, Thermo scientific) overnight. Cells were then fixed in 2% paraformaldehyde (PFA), permeabilized with 0.1% Triton X-100, and blocked with 3% normal donkey serum (NDS) in PBS. Cells were stained with primary antibodies and washed twice with PBST and visualized with fluorescent-dye conjugated secondary antibodies.

PLA assay was performed as previously described to detect NLRC4-NLRP3 proximity (76). Human RPE cells were plated in an 8-well chamber slide overnight. Cells were stimulated and then fixed in 2% PFA, permeabilized with 0.1% Triton X-100, and blocked with 3% NDS. Slides were incubated overnight with primary antibodies prepared in antibody diluent.

Signals were visualized with fluorescent red detection reagent kit. Fluorescence images were captured by Nikon A1R laser scanning confocal microscope, and bright field images by Olympus slide scanning microscope.

Fluorescence in situ hybridization and Immunofluorescence staining

To prepare the Digoxigenin (DIG) labelled *Alu* RNA probes, the DNA templates were amplified with T7 promoter containing primers and DIG-labelled RNA probes were transcribed using the DIG RNA Labeling Kit (11175025910, Sigma) from DNA templates. RNA probes were purified using MEGAclear (Ambion) and validated using anti-DIG dot blotting.

Primary PBMCs were plated in an 8-well chamber slide (154941, Thermo scientific) overnight. The attached cells were raised with pre-chilled PBS and fixed in 4% paraformaldehyde (PFA). Permeabilize PBMCs with 0.2 % Triton X-100, and then wash with 1xSSC and blocked with hybridization buffer (50% formamide, 5x SSC, 0.1% Tween-20, 0.5% SDS, 500 μg/ml tRNA, 500 μg/ml salmon sperm DNA, 50 μg/ml heparin salt) at 60 °C. The PBMCs were hybridized with 200 ng of DIG-labeled *Alu* RNA probes in hybridization buffer at 60 °C for 16 h. After hybridization, the cells were washed twice (5x SSC, 0.1% Tween-20) at 60 °C, and then blocked with blocking buffer (1x PBS, 5% NGS, 0.2% Triton X-100) and incubated with primary antibodies (Anti-DIG, MAB7520, R&D Systems; Anti-DDX17, A300-509A, Bethyl Laboratories) at 4 °C overnight. Next day, PBMCs were washed twice with PBST and visualized with fluorescent dye conjugated secondary antibodies.

Nuclear and cytoplasmic fractionation

Cytoplasmic and nuclear protein separation were performed using the NE-PER™ Nuclear and Cytoplasmic Extraction Kit. Briefly, THP-1 cells were stimulated with *Alu* RNA for 12 h, and cells were collected and lysed with ice cold CER I for 15 min on ice. Lysates were vortexed and centrifuged at 1,000g for 10 min at 4 °C. Lysates were resuspended in ice-cold CER II, vortexed and centrifuged to collect the supernatant as cytoplasmic extract. The pellet was resuspended with ice-cold NER vortexed and further centrifuged for 10 min at 13,000g at room temperature. Lysate supernatant was used as the nuclear fraction.

Real-time PCR

Total RNA was extracted from cells using the TRIzol reagent (15596026, Invitrogen) according to the manufacturer's instructions. cDNA was synthesized using a QuantiTect Reverse Transcription kit (205313, QIAGEN). Target genes were amplified by real-time quantitative PCR (Applied Biosystems 7900 HT Fast Real-Time PCR system) with Power SYBR green Master Mix. Relative gene expression was determined by the $2^{-\Delta\Delta Ct}$ method, and 18S rRNA or GAPDH was used as an internal control.

Northern blotting

Total RNA was extracted with primary PMBCs or BMDMs using the TRIzol reagent (15596026, Invitrogen) according to the manufacturer's instructions. Equal amounts of total RNA from different groups were mixed with 2x TBE-Urea Sample Buffer, heated at

50 °C for 5 min, and kept on ice. Then, RNA samples and Biotinylated sRNA Ladder were electrophoresed on 10% Novex™ TBE-Urea Gels and transferred on to Hybond-N membrane. The loaded membrane was crosslinked using ultraviolet light and prehybridized with hybridization buffer (50% Formamide, 5x SSC, 0.1% SDS, 200 μg/ml Herring sperm DNA, 5 mM EDTA) at 60 °C for 30 min, and then hybridized with *Alu*, B2 RNA and 5S rRNA probes at 42 °C overnight. The next day, the membrane was washed with washing buffer (1xSSC, 1% SDS) at 42 °C three times, and then developed with the Chemiluminescent Nucleic Acid Detection Module Kit.

Immunoblotting

Cells and tissue were homogenized in RIPA buffer (R0278, Sigma) with protease and phosphatase inhibitors (A32959, Thermo Scientific). Protein concentration was determined with a Pierce BCA Protein Assay Kit (23225, Thermo Scientific). Equal quantities of protein boiled in LDS Sample Buffer (NP0007, Thermo Scientific) were resolved by Novex Tris-glycine gels (Invitrogen) and transferred onto LF PVDF membranes (1704274, Bio-Rad).

For NATIVE PAGE, Cells were washed once with pre-chilled PBS and then lysed in ice-cold native lysis buffer (20 mM Tris-HCL, 20 mM NaCl, 10% (w/v) glycerol, 0.5% digitonin, 0.5 mM Na_3VO_4, 1 mM PMSF, 0.5 mM NaF, 1×Roche protease inhibitor cocktail, pH 7.5) for 30 min on ice. Cell lysates were centrifuged for 30 min at 12,000 rpm at 4 °C. Protein concentration was determined by Pierce BCA Protein Assay Kit. Equal quantities of protein were prepared in Native Sample Buffer (LC2673, Thermo Scientific) and resolved by 4–12% Native Tris-glycine gels. Native gels were incubated in 10% SDS solution for 5 min and transferred on to LF PVDF membranes. The transferred membranes were blocked with Blocking Buffer (927–40000, LI-COR) and incubated with the following primary antibodies. The signal was visualized with species-specific secondary antibodies conjugated with IRDye and Odyssey® CLx Imaging System.

Subretinal injection and fundus photography

Subretinal injections of SINE RNAs in mice were performed as previously described (14). 1 μl of cholesterol-conjugated siRNA (2 μg/μl) targeting mouse *Ddx17* or *Luc* were delivered as intravitreous injections three days prior to *Alu* RNA administration. The eye used for active versus control injection was chosen randomly. 7 days after SINE RNA injection, fundus photographs of dilated mouse eyes were captured by TRC-50 IX camera (Topcon) linked to a digital imaging system (Sony).

Assessment of RPE degeneration

RPE health was assessed by fundus photography and immunofluorescence staining of zonula occludens-1 (ZO-1) on RPE flat mounts as previously described (14). Quantification of RPE degeneration was performed as previously described (14) by using two methods (binary assignment and cellular morphometry). Binary assignment (healthy versus unhealthy) was independently performed by two masked observers (inter-rater agreement = 100%; Pearson $r^2 = 1.0$, $P < 0.0001$; Fleiss $\kappa = 1.0$, $P < 0.0001$). Quantifying cellular morphometry for tessellated cells was performed in semi-automated fashion with Konan Cell Check software (Ver. 4.0.1) by two masked graders.

Quantification and statistical analysis

The binary readouts of RPE degeneration (i.e., the presence or absence of RPE degeneration on fundus and ZO-1-stained flat-mount images) were analyzed with Fisher's exact test. Cell-morphometry data were assessed with two-tailed Mann-Whitney U test. Sample sizes were selected on the basis of power analysis with $\alpha = 5\%$ and $1 - \beta = 80\%$, such that we were able to detect a minimum of 50% change, assuming a sample s.d. based on Bayesian inference. Outliers were assessed with Grubbs' test. Based on this analysis, no outliers were detected, and no data were excluded. Fewer than 5% of subretinal-injection recipient tissues were excluded based on predetermined exclusion criteria (including hemorrhage and animal death due to anesthesia complications) relating to the technical challenges of this delicate procedure. All other data were expressed as mean ± SEM and were analyzed with unpaired two-sided t test, one-way ANOVA with Dunnett's multiple comparisons, or two-way ANOVA with Sidak's multiple comparisons test. P values < 0.05 were deemed statistically significant.

Supplementary Material

Refer to Web version on PubMed Central for supplementary material.

Acknowledgments:

We thank Russell E. Vance and Isabella Rauch for detailed discussions on the manuscript. We also thank Douglas L. Black, Peter Tontonoz, Gabriel Nuñez, Ghanshyam Swarup, and Russell E. Vance for providing mice and reagents, and D. Robertson, K. Langberg, J. Hu, G. Pattison, K.A. Fox, and C. Spee for technical assistance.

Funding:

J.A. has received support from NIH grants (DP1GM114862, R01EY028027, R01EY29799, R01EY031039), John Templeton Foundation Grant 60763, the UVA Strategic Investment Fund, DuPont Guerry, III, Professorship, and a gift from Mr. and Mrs. Eli W. Tullis; N.K. by NIH (R01AI148741, R00EY024336, R21EY030651); B.D.G. has received support from NIH grants (R01EY028027, R01EY031039, R01EY032512), BrightFocus Foundation, and the Owens Family Foundation.

REFERENCES AND NOTES

1. Deininger P, Alu elements: know the SINEs. Genome Biol 12, 236 (2011). [PubMed: 22204421]
2. Ullu E, Tschudi C, Alu sequences are processed 7SL RNA genes. Nature 312, 171–172 (1984). [PubMed: 6209580]
3. Roy AM, Gong C, Kass DH, Deininger PL, Recent B2 element insertions in the mouse genome. DNA Seq 8, 343–348 (1998). [PubMed: 10993604]
4. Kazazian HH Jr., Moran JV, Mobile DNA in Health and Disease. N Engl J Med 377, 361–370 (2017). [PubMed: 28745987]
5. Schaller AM, Tucker J, Willis I, Glaunsinger BA, Conserved Herpesvirus Kinase ORF36 Activates B2 Retrotransposons during Murine Gammaherpesvirus Infection. J Virol 94, e00262–00220 (2020). [PubMed: 32404524]
6. Maxwell PH, Burhans WC, Curcio MJ, Retrotransposition is associated with genome instability during chronological aging. Proc Natl Acad Sci U S A 108, 20376–20381 (2011). [PubMed: 22021441]
7. De Cecco M, Criscione SW, Peterson AL, Neretti N, Sedivy JM, Kreiling JA, Transposable elements become active and mobile in the genomes of aging mammalian somatic tissues. Aging (Albany NY) 5, 867–883 (2013). [PubMed: 24323947]

8. Kaneko H, Dridi S, Tarallo V, Gelfand BD, Fowler BJ, Cho WG, Kleinman ME, Ponicsan SL, Hauswirth WW, Chiodo VA, Kariko K, Yoo JW, Lee DK, Hadziahmetovic M, Song Y, Misra S, Chaudhuri G, Buaas FW, Braun RE, Hinton DR, Zhang Q, Grossniklaus HE, Provis JM, Madigan MC, Milam AH, Justice NL, Albuquerque RJ, Blandford AD, Bogdanovich S, Hirano Y, Witta J, Fuchs E, Littman DR, Ambati BK, Rudin CM, Chong MM, Provost P, Kugel JF, Goodrich JA, Dunaief JL, Baffi JZ, Ambati J, DICER1 deficit induces Alu RNA toxicity in age-related macular degeneration. Nature 471, 325–330 (2011). [PubMed: 21297615]
9. Guo C, Jeong HH, Hsieh YC, Klein HU, Bennett DA, De Jager PL, Liu Z, Shulman JM, Tau Activates Transposable Elements in Alzheimer's Disease. Cell Rep 23, 2874–2880 (2018). [PubMed: 29874575]
10. Cheng Y, Saville L, Gollen B, Isaac C, Belay A, Mehla J, Patel K, Thakor N, Mohajerani MH, Zovoilis A, Increased processing of SINE B2 ncRNAs unveils a novel type of transcriptome deregulation in amyloid beta neuropathology. Elife 9, e61265 (2020). [PubMed: 33191914]
11. Heinrich MJ, Purcell CA, Pruijssers AJ, Zhao Y, Spurlock CF 3rd, Sriram S, Ogden KM, Dermody TS, Scholz MB, Crooke PS 3rd, Karijolich J, Aune TM, Endogenous double-stranded Alu RNA elements stimulate IFN-responses in relapsing remitting multiple sclerosis. J Autoimmun 100, 40–51 (2019). [PubMed: 30826177]
12. Ambati J, Magagnoli J, Leung H, Wang SB, Andrews CA, Fu D, Pandey A, Sahu S, Narendran S, Hirahara S, Fukuda S, Sun J, Pandya L, Ambati M, Pereira F, Varshney A, Cummings T, Hardin JW, Edun B, Bennett CL, Ambati K, Fowler BJ, Kerur N, Rover C, Leitinger N, Werner BC, Stein JD, Sutton SS, Gelfand BD, Repurposing anti-inflammasome NRTIs for improving insulin sensitivity and reducing type 2 diabetes development. Nat Commun 11, 4737 (2020). [PubMed: 32968070]
13. Hung T, Pratt GA, Sundararaman B, Townsend MJ, Chaivorapol C, Bhangale T, Graham RR, Ortmann W, Criswell LA, Yeo GW, Behrens TW, The Ro60 autoantigen binds endogenous retroelements and regulates inflammatory gene expression. Science 350, 455–459 (2015). [PubMed: 26382853]
14. Tarallo V, Hirano Y, Gelfand BD, Dridi S, Kerur N, Kim Y, Cho WG, Kaneko H, Fowler BJ, Bogdanovich S, Albuquerque RJ, Hauswirth WW, Chiodo VA, Kugel JF, Goodrich JA, Ponicsan SL, Chaudhuri G, Murphy MP, Dunaief JL, Ambati BK, Ogura Y, Yoo JW, Lee DK, Provost P, Hinton DR, Nunez G, Baffi JZ, Kleinman ME, Ambati J, DICER1 loss and Alu RNA induce age-related macular degeneration via the NLRP3 inflammasome and MyD88. Cell 149, 847–859 (2012). [PubMed: 22541070]
15. Broz P, Dixit VM, Inflammasomes: mechanism of assembly, regulation and signalling. Nat Rev Immunol 16, 407–420 (2016). [PubMed: 27291964]
16. Davis BK, Wen H, Ting JP, The inflammasome NLRs in immunity, inflammation, and associated diseases. Annu Rev Immunol 29, 707–735 (2011). [PubMed: 21219188]
17. He Y, Hara H, Nunez G, Mechanism and Regulation of NLRP3 Inflammasome Activation. Trends Biochem Sci 41, 1012–1021 (2016). [PubMed: 27669650]
18. Duncan JA, Canna SW, The NLRC4 Inflammasome. Immunol Rev 281, 115–123 (2018). [PubMed: 29247997]
19. Rauch I, Tenthorey JL, Nichols RD, Al Moussawi K, Kang JJ, Kang C, Kazmierczak BI, Vance RE, NAIP proteins are required for cytosolic detection of specific bacterial ligands in vivo. J Exp Med 213, 657–665 (2016). [PubMed: 27045008]
20. He Y, Zeng MY, Yang D, Motro B, Nunez G, NEK7 is an essential mediator of NLRP3 activation downstream of potassium efflux. Nature 530, 354–357 (2016). [PubMed: 26814970]
21. Sharif H, Wang L, Wang WL, Magupalli VG, Andreeva L, Qiao Q, Hauenstein AV, Wu Z, Nunez G, Mao Y, Wu H, Structural mechanism for NEK7-licensed activation of NLRP3 inflammasome. Nature 570, 338–343 (2019). [PubMed: 31189953]
22. Verma V, Gupta S, Kumar P, Yadav S, Dhanda RS, Gaind R, Arora R, Frimodt-Moller N, Yadav M, Involvement of NLRP3 and NLRC4 Inflammasome in Uropathogenic E. coli Mediated Urinary Tract Infections. Front Microbiol 10, 2020 (2019). [PubMed: 31551961]
23. Gram AM, Wright JA, Pickering RJ, Lam NL, Booty LM, Webster SJ, Bryant CE, Salmonella Flagellin Activates NAIP/NLRC4 and Canonical NLRP3 Inflammasomes in Human Macrophages. J Immunol 206, 631–640 (2021). [PubMed: 33380493]

24. Broz P, Newton K, Lamkanfi M, Mariathasan S, Dixit VM, Monack DM, Redundant roles for inflammasome receptors NLRP3 and NLRC4 in host defense against Salmonella. J Exp Med 207, 1745–1755 (2010). [PubMed: 20603313]
25. Chen H, Deng Y, Gan X, Li Y, Huang W, Lu L, Wei L, Su L, Luo J, Zou B, Hong Y, Cao Y, Liu Y, Chi W, NLRP12 collaborates with NLRP3 and NLRC4 to promote pyroptosis inducing ganglion cell death of acute glaucoma. Mol Neurodegener 15, 26 (2020). [PubMed: 32295623]
26. Freeman L, Guo H, David CN, Brickey WJ, Jha S, Ting JP, NLR members NLRC4 and NLRP3 mediate sterile inflammasome activation in microglia and astrocytes. J Exp Med 214, 1351–1370 (2017). [PubMed: 28404595]
27. Koh EH, Yoon JE, Ko MS, Leem J, Yun JY, Hong CH, Cho YK, Lee SE, Jang JE, Baek JY, Yoo HJ, Kim SJ, Sung CO, Lim JS, Jeong WI, Back SH, Baek IJ, Torres S, Solsona-Vilarrasa E, Conde de la Rosa L, Garcia-Ruiz C, Feldstein AE, Fernandez-Checa JC, Lee KU, Sphingomyelin synthase 1 mediates hepatocyte pyroptosis to trigger non-alcoholic steatohepatitis. Gut, (2020).
28. Ip WK, Medzhitov R, Macrophages monitor tissue osmolarity and induce inflammatory response through NLRP3 and NLRC4 inflammasome activation. Nat Commun 6, 6931 (2015). [PubMed: 25959047]
29. Qu Y, Misaghi S, Newton K, Maltzman A, Izrael-Tomasevic A, Arnott D, Dixit VM, NLRP3 recruitment by NLRC4 during Salmonella infection. J Exp Med 213, 877–885 (2016). [PubMed: 27139490]
30. Man SM, Hopkins LJ, Nugent E, Cox S, Gluck IM, Tourlomousis P, Wright JA, Cicuta P, Monie TP, Bryant CE, Inflammasome activation causes dual recruitment of NLRC4 and NLRP3 to the same macromolecular complex. Proc Natl Acad Sci U S A 111, 7403–7408 (2014). [PubMed: 24803432]
31. Tenthorey JL, Haloupek N, Lopez-Blanco JR, Grob P, Adamson E, Hartenian E, Lind NA, Bourgeois NM, Chacon P, Nogales E, Vance RE, The structural basis of flagellin detection by NAIP5: A strategy to limit pathogen immune evasion. Science 358, 888–893 (2017). [PubMed: 29146805]
32. Zhang L, Chen S, Ruan J, Wu J, Tong AB, Yin Q, Li Y, David L, Lu A, Wang WL, Marks C, Ouyang Q, Zhang X, Mao Y, Wu H, Cryo-EM structure of the activated NAIP2-NLRC4 inflammasome reveals nucleated polymerization. Science 350, 404–409 (2015). [PubMed: 26449474]
33. Furman D, Chang J, Lartigue L, Bolen CR, Haddad F, Gaudilliere B, Ganio EA, Fragiadakis GK, Spitzer MH, Douchet I, Daburon S, Moreau JF, Nolan GP, Blanco P, Dechanet-Merville J, Dekker CL, Jojic V, Kuo CJ, Davis MM, Faustin B, Expression of specific inflammasome gene modules stratifies older individuals into two extreme clinical and immunological states. Nat Med 23, 174–184 (2017). [PubMed: 28092664]
34. Poh L, Kang SW, Baik SH, Ng GYQ, She DT, Balaganapathy P, Dheen ST, Magnus T, Gelderblom M, Sobey CG, Koo EH, Fann DY, Arumugam TV, Evidence that NLRC4 inflammasome mediates apoptotic and pyroptotic microglial death following ischemic stroke. Brain Behav Immun 75, 34–47 (2019). [PubMed: 30195027]
35. Qu Y, Misaghi S, Izrael-Tomasevic A, Newton K, Gilmour LL, Lamkanfi M, Louie S, Kayagaki N, Liu J, Komuves L, Cupp JE, Arnott D, Monack D, Dixit VM, Phosphorylation of NLRC4 is critical for inflammasome activation. Nature 490, 539–542 (2012). [PubMed: 22885697]
36. Matusiak M, Van Opdenbosch N, Vande Walle L, Sirard JC, Kanneganti TD, Lamkanfi M, Flagellin-induced NLRC4 phosphorylation primes the inflammasome for activation by NAIP5. Proc Natl Acad Sci U S A 112, 1541–1546 (2015). [PubMed: 25605939]
37. Liu W, Liu X, Li Y, Zhao J, Liu Z, Hu Z, Wang Y, Yao Y, Miller AW, Su B, Cookson MR, Li X, Kang Z, LRRK2 promotes the activation of NLRC4 inflammasome during Salmonella Typhimurium infection. J Exp Med 214, 3051–3066 (2017). [PubMed: 28821568]
38. Hu Z, Zhou Q, Zhang C, Fan S, Cheng W, Zhao Y, Shao F, Wang HW, Sui SF, Chai J, Structural and biochemical basis for induced self-propagation of NLRC4. Science 350, 399–404 (2015). [PubMed: 26449475]
39. Miao EA, Leaf IA, Treuting PM, Mao DP, Dors M, Sarkar A, Warren SE, Wewers MD, Aderem A, Caspase-1-induced pyroptosis is an innate immune effector mechanism against intracellular bacteria. Nat Immunol 11, 1136–1142 (2010). [PubMed: 21057511]

40. Aglietti RA, Estevez A, Gupta A, Ramirez MG, Liu PS, Kayagaki N, Ciferri C, Dixit VM, Dueber EC, GsdmD p30 elicited by caspase-11 during pyroptosis forms pores in membranes. Proc Natl Acad Sci U S A 113, 7858–7863 (2016). [PubMed: 27339137]
41. Shi J, Zhao Y, Wang K, Shi X, Wang Y, Huang H, Zhuang Y, Cai T, Wang F, Shao F, Cleavage of GSDMD by inflammatory caspases determines pyroptotic cell death. Nature 526, 660–665 (2015). [PubMed: 26375003]
42. Kerur N, Fukuda S, Banerjee D, Kim Y, Fu D, Apicella I, Varshney A, Yasuma R, Fowler BJ, Baghdasaryan E, Marion KM, Huang X, Yasuma T, Hirano Y, Serbulea V, Ambati M, Ambati VL, Kajiwara Y, Ambati K, Hirahara S, Bastos-Carvalho A, Ogura Y, Terasaki H, Oshika T, Kim KB, Hinton DR, Leitinger N, Cambier JC, Buxbaum JD, Kenney MC, Jazwinski SM, Nagai H, Hara I, West AP, Fitzgerald KA, Sadda SR, Gelfand BD, Ambati J, cGAS drives noncanonical-inflammasome activation in age-related macular degeneration. Nat Med 24, 50–61 (2018). [PubMed: 29176737]
43. Bulek K, Zhao J, Liao Y, Rana N, Corridoni D, Antanaviciute A, Chen X, Wang H, Qian W, Miller-Little WA, Swaidani S, Tang F, Willard BB, McCrae K, Kang Z, Dubyak GR, Cominelli F, Simmons A, Pizarro TT, Li X, Epithelial-derived gasdermin D mediates nonlytic IL-1beta release during experimental colitis. J Clin Invest 130, 4218–4234 (2020). [PubMed: 32597834]
44. Tenthorey JL, Chavez RA, Thompson TW, Deets KA, Vance RE, Rauch I, NLRC4 inflammasome activation is NLRP3- and phosphorylation-independent during infection and does not protect from melanoma. J Exp Med 217, (2020).
45. Kofoed EM, Vance RE, Innate immune recognition of bacterial ligands by NAIPs determines inflammasome specificity. Nature 477, 592–595 (2011). [PubMed: 21874021]
46. Zhao Y, Yang J, Shi J, Gong YN, Lu Q, Xu H, Liu L, Shao F, The NLRC4 inflammasome receptors for bacterial flagellin and type III secretion apparatus. Nature 477, 596–600 (2011). [PubMed: 21918512]
47. Reyes Ruiz VM, Ramirez J, Naseer N, Palacio NM, Siddarthan IJ, Yan BM, Boyer MA, Pensinger DA, Sauer JD, Shin S, Broad detection of bacterial type III secretion system and flagellin proteins by the human NAIP/NLRC4 inflammasome. Proc Natl Acad Sci U S A 114, 13242–13247 (2017). [PubMed: 29180436]
48. Yang J, Zhao Y, Shi J, Shao F, Human NAIP and mouse NAIP1 recognize bacterial type III secretion needle protein for inflammasome activation. Proc Natl Acad Sci U S A 110, 14408–14413 (2013). [PubMed: 23940371]
49. Miao EA, Alpuche-Aranda CM, Dors M, Clark AE, Bader MW, Miller SI, Aderem A, Cytoplasmic flagellin activates caspase-1 and secretion of interleukin 1beta via Ipaf. Nat Immunol 7, 569–575 (2006). [PubMed: 16648853]
50. Yim HC, Wang D, Yu L, White CL, Faber PW, Williams BR, Sadler AJ, The kinase activity of PKR represses inflammasome activity. Cell Res 26, 367–379 (2016). [PubMed: 26794869]
51. Chu WM, Ballard R, Carpick BW, Williams BR, Schmid CW, Potential Alu function: regulation of the activity of double-stranded RNA-activated kinase PKR. Mol Cell Biol 18, 58–68 (1998). [PubMed: 9418853]
52. Moy RH, Cole BS, Yasunaga A, Gold B, Shankarling G, Varble A, Molleston JM, tenOever BR, Lynch KW, Cherry S, Stem-loop recognition by DDX17 facilitates miRNA processing and antiviral defense. Cell 158, 764–777 (2014). [PubMed: 25126784]
53. Sand J, Haertel E, Biedermann T, Contassot E, Reichmann E, French LE, Werner S, Beer HD, Expression of inflammasome proteins and inflammasome activation occurs in human, but not in murine keratinocytes. Cell Death Dis 9, 24 (2018). [PubMed: 29348630]
54. Gelfand BD, Wright CB, Kim Y, Yasuma T, Yasuma R, Li S, Fowler BJ, Bastos-Carvalho A, Kerur N, Uittenbogaard A, Han YS, Lou D, Kleinman ME, McDonald WH, Nunez G, Georgel P, Dunaief JL, Ambati J, Iron Toxicity in the Retina Requires Alu RNA and the NLRP3 Inflammasome. Cell Rep 11, 1686–1693 (2015). [PubMed: 26074074]
55. Wright CB, Uehara H, Kim Y, Yasuma T, Yasuma R, Hirahara S, Makin RD, Apicella I, Pereira F, Nagasaka Y, Narendran S, Fukuda S, Albuquerque R, Fowler BJ, Bastos-Carvalho A, Georgel P, Hatada I, Chang B, Kerur N, Ambati BK, Ambati J, Gelfand BD, Chronic Dicer1 deficiency promotes atrophic and neovascular outer retinal pathologies in mice. Proc Natl Acad Sci U S A 117, 2579–2587 (2020). [PubMed: 31964819]

56. Bossu P, Neumann D, Del Giudice E, Ciaramella A, Gloaguen I, Fantuzzi G, Dinarello CA, Di Carlo E, Musiani P, Meroni PL, Caselli G, Ruggiero P, Boraschi D, IL-18 cDNA vaccination protects mice from spontaneous lupus-like autoimmune disease. Proc Natl Acad Sci U S A 100, 14181–14186 (2003). [PubMed: 14615579]
57. Mende R, Vincent FB, Kandane-Rathnayake R, Koelmeyer R, Lin E, Chang J, Hoi AY, Morand EF, Harris J, Lang T, Analysis of Serum Interleukin (IL)-1beta and IL-18 in Systemic Lupus Erythematosu. Front Immunol 9, 1250 (2018). [PubMed: 29930551]
58. Tomalka J, Ganesan S, Azodi E, Patel K, Majmudar P, Hall BA, Fitzgerald KA, Hise AG, A novel role for the NLRC4 inflammasome in mucosal defenses against the fungal pathogen Candida albicans. PLoS Pathog 7, e1002379 (2011). [PubMed: 22174673]
59. Wang X, Shaw DK, Hammond HL, Sutterwala FS, Rayamajhi M, Shirey KA, Perkins DJ, Bonventre JV, Velayutham TS, Evans SM, Rodino KG, VieBrock L, Scanlon KM, Carbonetti NH, Carlyon JA, Miao EA, McBride JW, Kotsyfakis M, Pedra JH, The Prostaglandin E2-EP3 Receptor Axis Regulates Anaplasma phagocytophilum-Mediated NLRC4 Inflammasome Activation. PLoS Pathog 12, e1005803 (2016). [PubMed: 27482714]
60. Suzuki S, Franchi L, He Y, Munoz-Planillo R, Mimuro H, Suzuki T, Sasakawa C, Nunez G, Shigella type III secretion protein MxiI is recognized by Naip2 to induce Nlrc4 inflammasome activation independently of Pkcdelta. PLoS Pathog 10, e1003926 (2014). [PubMed: 24516390]
61. Bezbradica JS, Coll RC, Schroder K, Sterile signals generate weaker and delayed macrophage NLRP3 inflammasome responses relative to microbial signals. Cell Mol Immunol 14, 118–126 (2017). [PubMed: 26996064]
62. Mitoma H, Hanabuchi S, Kim T, Bao M, Zhang Z, Sugimoto N, Liu YJ, The DHX33 RNA helicase senses cytosolic RNA and activates the NLRP3 inflammasome. Immunity 39, 123–135 (2013). [PubMed: 23871209]
63. Li J, Hu L, Liu Y, Huang L, Mu Y, Cai X, Weng C, DDX19A Senses Viral RNA and Mediates NLRP3-Dependent Inflammasome Activation. J Immunol 195, 5732–5749 (2015). [PubMed: 26538395]
64. Samir P, Kesavardhana S, Patmore DM, Gingras S, Malireddi RKS, Karki R, Guy CS, Briard B, Place DE, Bhattacharya A, Sharma BR, Nourse A, King SV, Pitre A, Burton AR, Pelletier S, Gilbertson RJ, Kanneganti TD, DDX3X acts as a live-or-die checkpoint in stressed cells by regulating NLRP3 inflammasome. Nature 573, 590–594 (2019). [PubMed: 31511697]
65. Zhu S, Ding S, Wang P, Wei Z, Pan W, Palm NW, Yang Y, Yu H, Li HB, Wang G, Lei X, de Zoete MR, Zhao J, Zheng Y, Chen H, Zhao Y, Jurado KA, Feng N, Shan L, Kluger Y, Lu J, Abraham C, Fikrig E, Greenberg HB, Flavell RA, Nlrp9b inflammasome restricts rotavirus infection in intestinal epithelial cells. Nature 546, 667–670 (2017). [PubMed: 28636595]
66. Wang P, Zhu S, Yang L, Cui S, Pan W, Jackson R, Zheng Y, Rongvaux A, Sun Q, Yang G, Gao S, Lin R, You F, Flavell R, Fikrig E, Nlrp6 regulates intestinal antiviral innate immunity. Science 350, 826–830 (2015). [PubMed: 26494172]
67. Li K, Mo C, Gong D, Chen Y, Huang Z, Li Y, Zhang J, Huang L, Li Y, Fuller-Pace FV, Lin P, Wei Y, DDX17 nucleocytoplasmic shuttling promotes acquired gefitinib resistance in non-small cell lung cancer cells via activation of beta-catenin. Cancer Lett 400, 194–202 (2017). [PubMed: 28259822]
68. Ngo TD, Partin AC, Nam Y, RNA Specificity and Autoregulation of DDX17, a Modulator of MicroRNA Biogenesis. Cell Rep 29, 4024–4035 e4025 (2019). [PubMed: 31851931]
69. Sun FJ, Fleurdepine S, Bousquet-Antonelli C, Caetano-Anolles G, Deragon JM, Common evolutionary trends for SINE RNA structures. Trends Genet 23, 26–33 (2007). [PubMed: 17126948]
70. Franchi L, Amer A, Body-Malapel M, Kanneganti TD, Ozoren N, Jagirdar R, Inohara N, Vandenabeele P, Bertin J, Coyle A, Grant EP, Nunez G, Cytosolic flagellin requires Ipaf for activation of caspase-1 and interleukin 1beta in salmonella-infected macrophages. Nat Immunol 7, 576–582 (2006). [PubMed: 16648852]
71. Kanneganti TD, Ozoren N, Body-Malapel M, Amer A, Park JH, Franchi L, Whitfield J, Barchet W, Colonna M, Vandenabeele P, Bertin J, Coyle A, Grant EP, Akira S, Nunez G, Bacterial RNA and small antiviral compounds activate caspase-1 through cryopyrin/Nalp3. Nature 440, 233–236 (2006). [PubMed: 16407888]

72. Miyamoto A, Nakayama K, Imaki H, Hirose S, Jiang Y, Abe M, Tsukiyama T, Nagahama H, Ohno S, Hatakeyama S, Nakayama KI, Increased proliferation of B cells and auto-immunity in mice lacking protein kinase Cdelta. Nature 416, 865–869 (2002). [PubMed: 11976687]

73. Weischenfeldt J, Porse B, Bone Marrow-Derived Macrophages (BMM): Isolation and Applications. CSH Protoc 2008, pdb prot5080 (2008).

74. Sallam T, Jones M, Thomas BJ, Wu X, Gilliland T, Qian K, Eskin A, Casero D, Zhang Z, Sandhu J, Salisbury D, Rajbhandari P, Civelek M, Hong C, Ito A, Liu X, Daniel B, Lusis AJ, Whitelegge J, Nagy L, Castrillo A, Smale S, Tontonoz P, Transcriptional regulation of macrophage cholesterol efflux and atherogenesis by a long noncoding RNA. Nat Med 24, 304–312 (2018). [PubMed: 29431742]

75. Sheu SJ, Sakamoto T, Osusky R, Wang HM, Ogden TE, Ryan SJ, Hinton DR, Gopalakrishna R, Transforming growth factor-beta regulates human retinal pigment epithelial cell phagocytosis by influencing a protein kinase C-dependent pathway. Graefes Arch Clin Exp Ophthalmol 232, 695–701 (1994). [PubMed: 7531168]

76. Barry R, John SW, Liccardi G, Tenev T, Jaco I, Chen CH, Choi J, Kasperkiewicz P, Fernandes-Alnemri T, Alnemri E, Drag M, Chen Y, Meier P, SUMO-mediated regulation of NLRP3 modulates inflammasome activity. Nat Commun 9, 3001 (2018). [PubMed: 30069026]

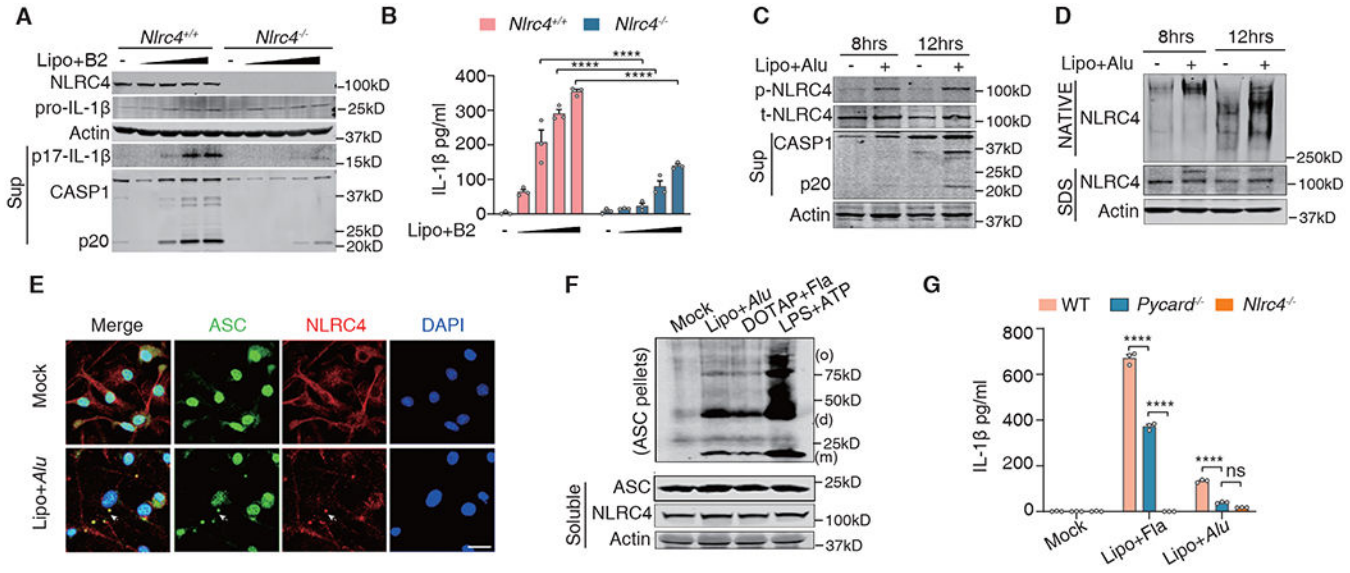

Fig. 1. SINE RNAs activate NLRC4 inflammasome.

(**A**) Immunoblot analysis of indicated proteins in cell lysates and supernatant of *Nlrc4*$^{+/+}$, *Nlrc4*$^{-/-}$ BMDMs transfected with various doses (25, 100, 250, 400 pmol) of B2 RNA or mock for 12 hours. “Mock” denotes the use of transfection reagents alone in all experiments. (**B**) ELISA quantification of IL-1β release from LPS-primed *Nlrc4*$^{+/+}$, *Nlrc4*$^{-/-}$ BMDMs transfected with various doses of B2 RNA or mock for 12 hours. “Lipo” represents lipofectamine 3000. (**C**) Immunoblot analysis of indicated proteins in BMDMs transfected with 100 pmol *Alu* RNA or mock at the indicated time points. (**D**) Immunoblot analysis of NLRC4 and actin, under native PAGE or SDS PAGE conditions, in BMDMs transfected with 100 pmol *Alu* RNA or mock at the indicated time points. (**E**) Confocal images of ASC specks and NLRC4 aggregates in 100pmol *Alu* RNA- or mock-transfected BMDMs. Scale bars, 20 μm. (**F**) Immunoblot analysis of ASC, NLRC4, and actin in cell lysates (soluble) and of ASC in DSS-crosslinked pellets (insoluble) with BMDM cells treated with LPS/ATP or transfected with *Alu* RNA (100 pmol) or flagellin (3 μg/ml, Fla). o, oligomers; d, dimers; m, monomers. (**G**) Measurement of IL-1β in LPS-primed wild-type (WT), *Pycard*$^{-/-}$ and *Nlrc4*$^{-/-}$ BMDMs transfected with 100 pmol *Alu* RNA for 12 hours or 3 μg/ml of flagellin (Fla) for 6 hours. Shown is the mean ± SEM for independent experiments. ****$P < 0.0001$; two-way ANOVA with Sidak’s multiple comparisons. ns, not significant.

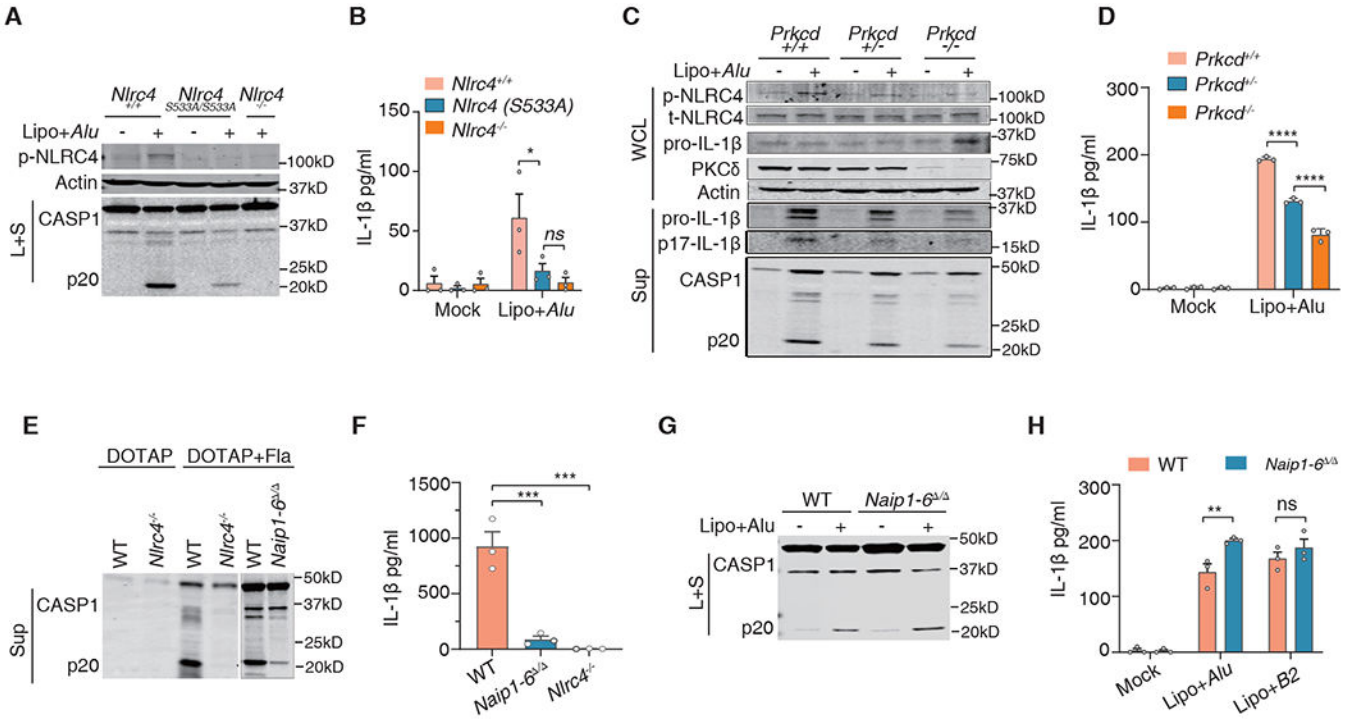

Fig. 2. NLRC4 phosphorylation (S533A) is important for SINE RNAs induced inflammasome activation.

(**A**) Primary BMDMs were isolated from *Nlrc4*$^{+/+}$, *Nlrc4*$^{S533A/S533A}$ and *Nlrc4*$^{-/-}$ mice, and transfected with 100 pmol *Alu* RNA or mock for 12 hours. The cell lysates were used for detecting phosphorylated NLRC4 (p-NLRC4) and actin; supernatant for pro-CASP1 (p45), cleaved CASP1 (p20) by immunoblotting. L+S, lysates and supernatant. (**B**) ELISA measurement of IL-1β release in LPS-primed *Nlrc4*$^{+/+}$, *Nlrc4*$^{S533A/S533A}$ and *Nlrc4*$^{-/-}$ BMDMs transfected with 100 pmol *Alu* RNA or mock for 12 hours. (**C**) Immunoblot analysis of indicated proteins in wild-type (*Prkcd*$^{+/+}$), *Prkcd*$^{+/-}$, and *Prkcd*$^{-/-}$ BMDMs transfected with 100 pmol of *Alu* RNA or mock. Sup (supernatant); WCL (whole cell lysates). (**D**) Measurement of IL-1β in LPS-primed wild-type (*Prkcd*$^{+/+}$), *Prkcd*$^{+/-}$, and *Prkcd*$^{-/-}$ BMDMs transfected with 100 pmol of *Alu* RNA or mock for 12 hours. (**E**) Immunoblot analysis of indicated proteins in wild-type (WT), *Nlrc4*$^{-/-}$, or *Naip1-6*$^{\Delta/\Delta}$ BMDMs transfected with flagellin (3 μg/ml) using DOTAP or the transfection reagent DOTAP alone. Sup (supernatant). (**F**) ELISA measurement of IL-1β in LPS-primed wild-type (WT), *Nlrc4*$^{-/-}$, or *Naip1-6*$^{\Delta/\Delta}$ BMDMs transfected with flagellin (3 μg/ml) using DOTAP. (**G**) Immunoblot analysis of pro-CASP1 (p45) and cleaved CASP1 (p20) in WT and *Naip1-6*$^{\Delta/\Delta}$ BMDMs transfected with 100 pmol of *Alu* RNA or mock. L+S, lysates and supernatant. (**H**) ELISA measurement of IL-1β in LPS-primed WT and *Naip1-6*$^{\Delta/\Delta}$ BMDMs transfected with 100 pmol *Alu* RNA, B2 RNA, or mock for 12 hours. Shown is the mean ± SEM for independent experiments. *$P < 0.05$; **$P < 0.01$; ****$P < 0.0001$; two-way ANOVA with Sidak's multiple comparisons (B, D, H); or one-way ANOVA with Dunnett's multiple comparisons (F). ns, not significant.

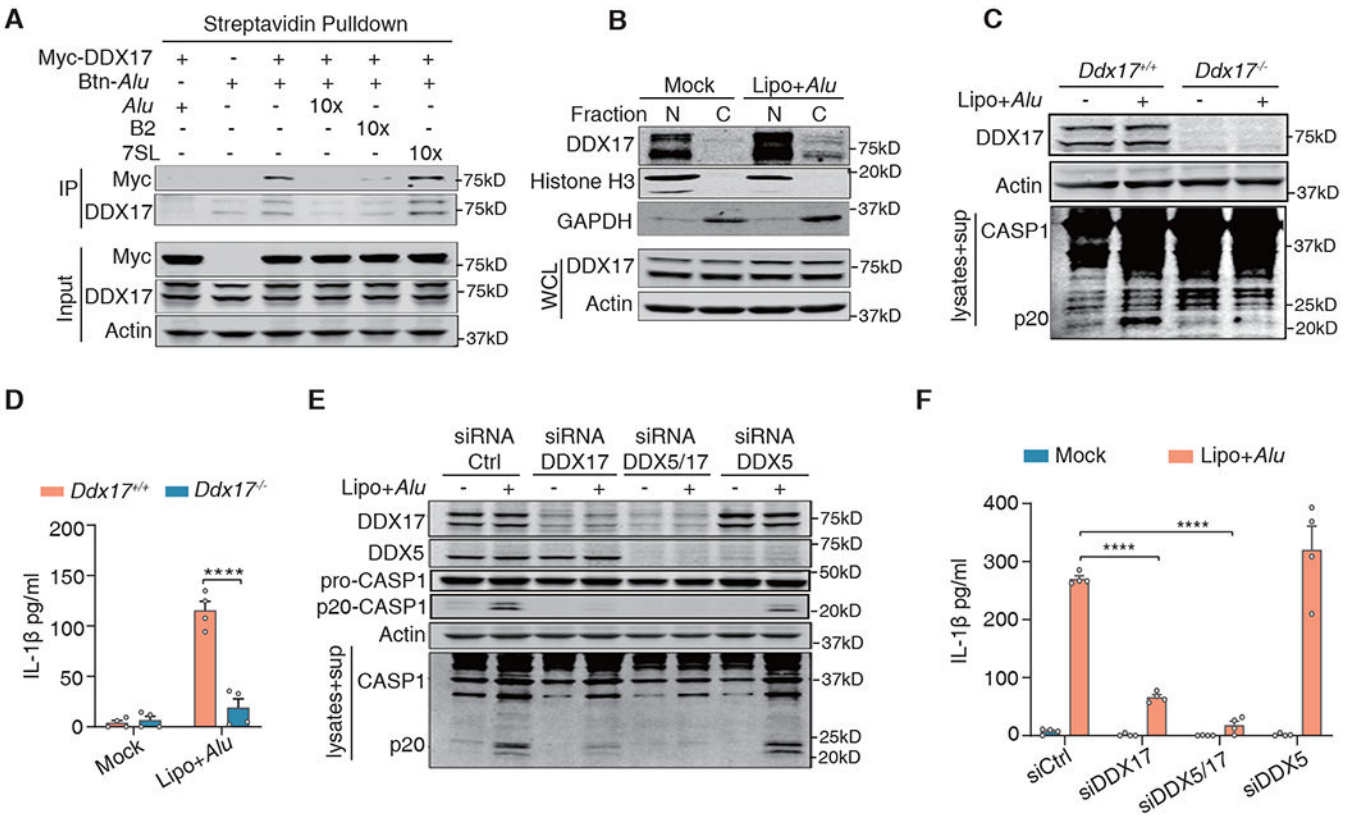

Fig. 3. DDX17 acts as the sensor of SINE RNA-induced NLRC4 inflammasome activation.

(**A**) Streptavidin affinity pull down of lysates of Myc-tagged DDX17-expressing HEK293T cells treated with biotin-labeled *Alu* RNA or label-free competitor RNAs as indicated, followed by immunoblot analysis of Myc, DDX17, and actin. (**B**) Immunoblot analysis of DDX17, histone H3, GAPDH and actin in cell fractions (N, nuclear; C, cytosol) and total lysates of THP-1 cells transfected with *Alu* RNA. WCL, whole cell lysate. (**C**) Immunoblot analysis of pro-CASP1 (p45), cleaved CASP1 (p20), DDX17, and actin in *Alu* RNA- or Mock-transfected *Ddx17*$^{+/+}$ and *Ddx17*$^{-/-}$ iBMDMs. (**D**) ELISA measurement of IL-1β secreted from LPS primed *Ddx17*$^{+/+}$ and *Ddx17*$^{-/-}$ iBMDMs transfected with 100 pmol of *Alu* RNA or mock for 12 hours. (**E**) Immunoblot analysis of pro-CASP1 (p45), cleaved CASP1 (p20), DDX17, DDX5, and actin in cell lysates from *Alu* RNA- or mock-transfected THP-1 cells pre-transfected with siRNA. Sup (supernatant). (**F**) ELISA measurement of IL-1β secreted from LPS primed THP-1 cells pre-transfected with siRNAs targeting DDX17, DDX5, or both, and then transfected with 100 pmol of *Alu* RNA or mock. Shown is the mean ± SEM for independent experiments. **** $P < 0.0001$; two-way ANOVA with Sidak's multiple comparisons.

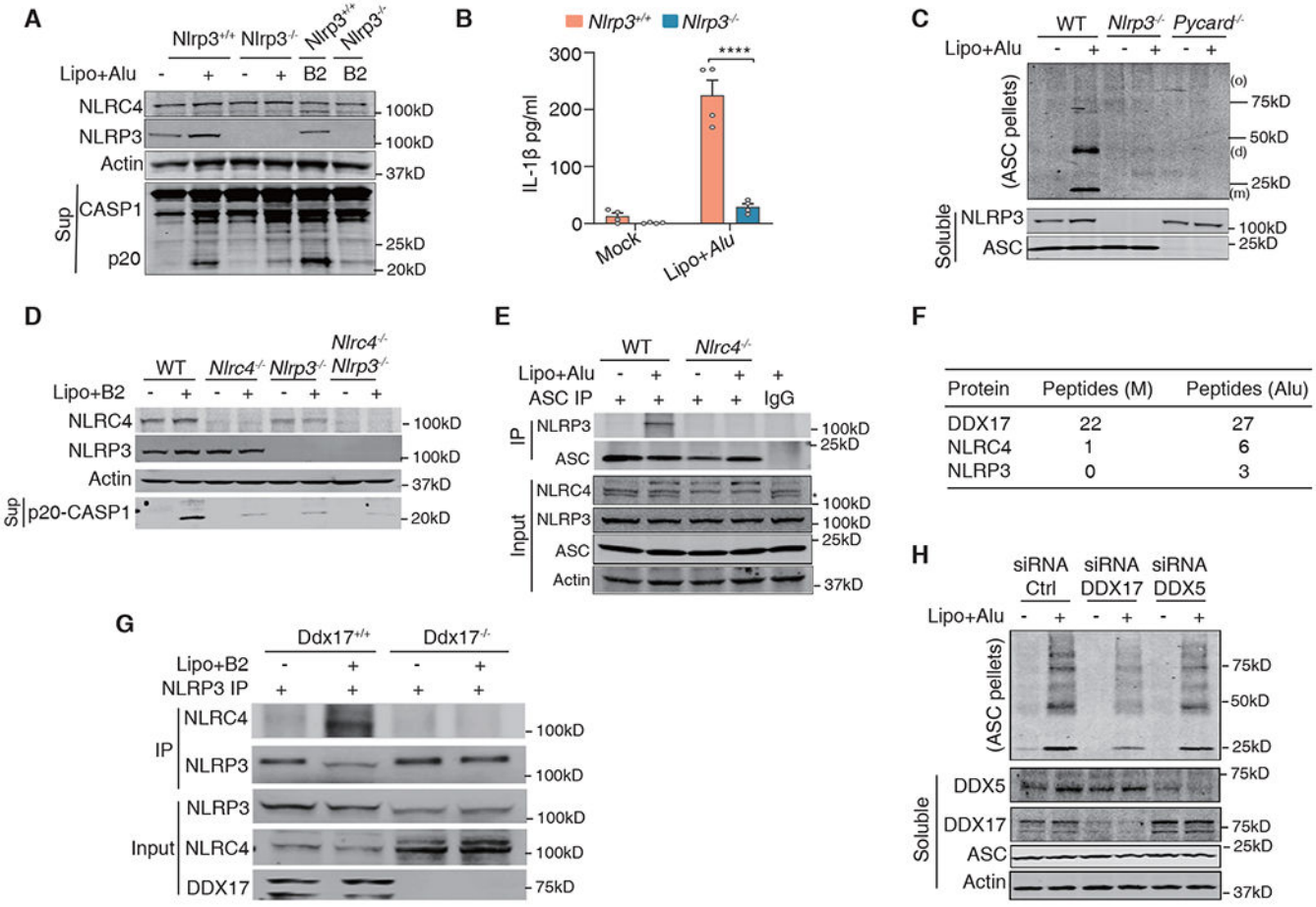

Fig. 4. DDX17 is required for sterile NLRC4/NLRP3 inflammasome assembly.

(**A**) Immunoblot analysis of indicated proteins in WT and *Nlrp3*$^{-/-}$ BMDMs transfected with 100 pmol of *Alu* RNA, B2 RNA, or mock. L+S, lysates and supernatant. (**B**). Measurement of IL-1β in LPS primed WT and *Nlrp3*$^{-/-}$ BMDMs transfected with 100 pmol of *Alu* RNA or mock. Shown is the mean ± SEM for independent experiments. **** $P < 0.0001$; two-way ANOVA with Sidak's multiple comparisons. (**C**) Immunoblot analysis of ASC and NLRP3 in cell lysates (soluble) and of ASC in DSS-crosslinked pellets (insoluble) in WT, *Nlrp3*$^{-/-}$, and *Pycard*$^{-/-}$ BMDMs transfected with 100 pmol of *Alu* RNA or mock. o, oligomers; d, dimers; m, monomers. (**D**) Immunoblot analysis of cleaved CASP1 (p20), NLRC4, NLRP3 and actin in cell lysates or supernatant of wild-type (WT), *Nlrc4*$^{-/-}$, *Nlrp3*$^{-/-}$, and *Nlrc4*$^{-/-}$ *Nlrp3*$^{-/-}$ primary BMDMs transfected with 100 pmol of B2 RNA or mock for 12 hours. (**E**) Co-immunoprecipitation (IP) of ASC and NLRP3 in WT and *Nlrc4*$^{-/-}$ BMDMs transfected with 100 pmol of *Alu* RNA or mock. * denotes the NLRC4 protein bands. (**F**) Mass spectrometry analysis of NLRC4 and NLRP3 peptides in purified DDX17-associated proteins. M, mock; Alu, *Alu* RNA. (**G**) Co-immunoprecipitation (IP) of NLRC4 and NLRP3 in *Ddx17*$^{+/+}$ and *Ddx17*$^{-/-}$ iBMDMs transfected with B2 RNA or Mock. (**H**) Immunoblot analysis of ASC, DDX5, DDX17, and actin in cell lysates (soluble) and of ASC in DSS-crosslinked pellets (insoluble) in THP-1 cells transfected with siRNAs

targeting DDX17, DDX5, or both and followed with transfection of 100 pmol of *Alu* RNA or mock for 12 hours.

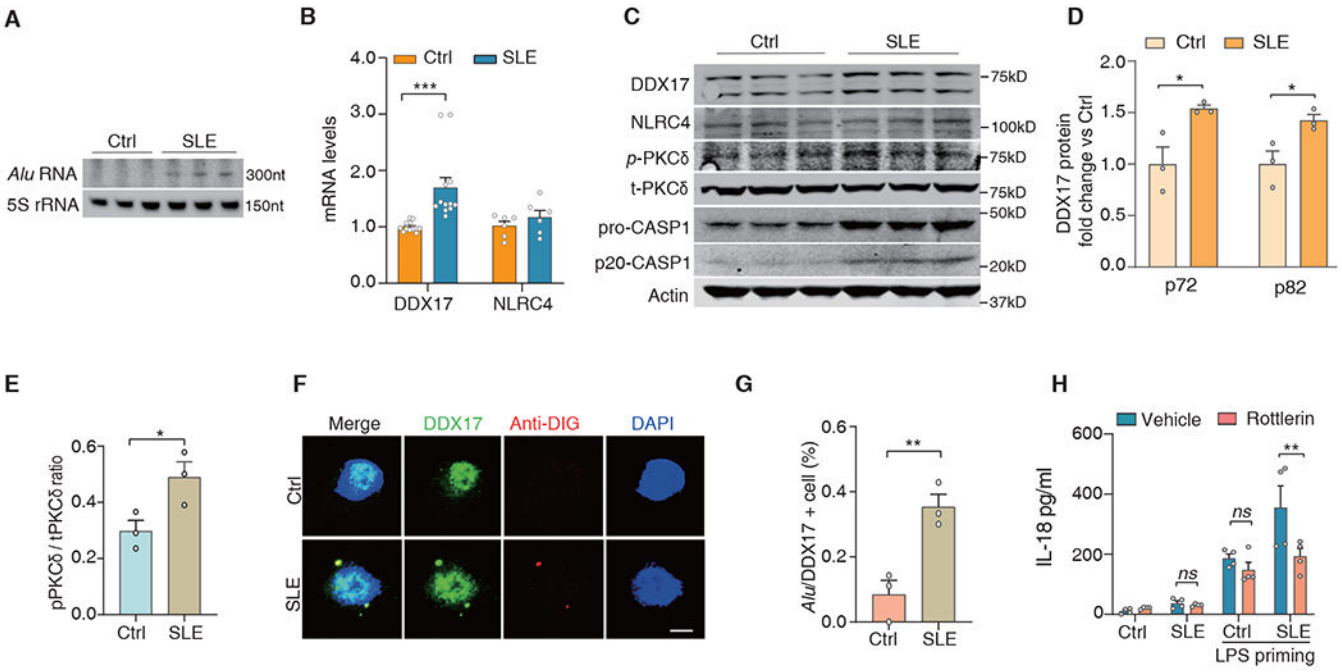

Fig. 5. Endogenous *Alu* RNA accumulation and sterile NLRC4 inflammasome activation in SLE PBMCs.

(**A**) Northern blot analysis of *Alu* RNA and 5S rRNA in primary PBMCs isolated from healthy control (Ctrl) and SLE patients. (**B**) Quantification of DDX17 and NLRC4 mRNA levels in primary PBMCs by RT-qPCR. (**C** to **E**) Immunoblot analysis of DDX17, NLRC4, p-PKCδ (Tyr311), total PKCδ (t-PKCδ), cleaved CASP1 (p20), and actin in primary PBMCs isolated from healthy control and SLE patients. Quantification of increased DDX17 expression (D) and PKCδ phosphorylation (E). (**F** and **G**) Immunofluorescence analysis and quantification of DDX17 and *Alu* RNA co-localization puncta in SLE PBMCs. Scale bars, 10 μm. (**H**) ELISA measurement of IL-18 secreted by primary PBMCs pre-treated with the PKC-δ inhibitor Rottlerin (5.0 μM) or vehicle, with or without LPS (250 ng/ml) priming. Shown is the mean ± SEM for independent experiments. *$P < 0.05$; **$P < 0.01$; ***$P <$ 0.001, two-way ANOVA with Sidak's multiple comparisons (B and H) or Unpaired *t* test (D, E, G). ns, not significant.

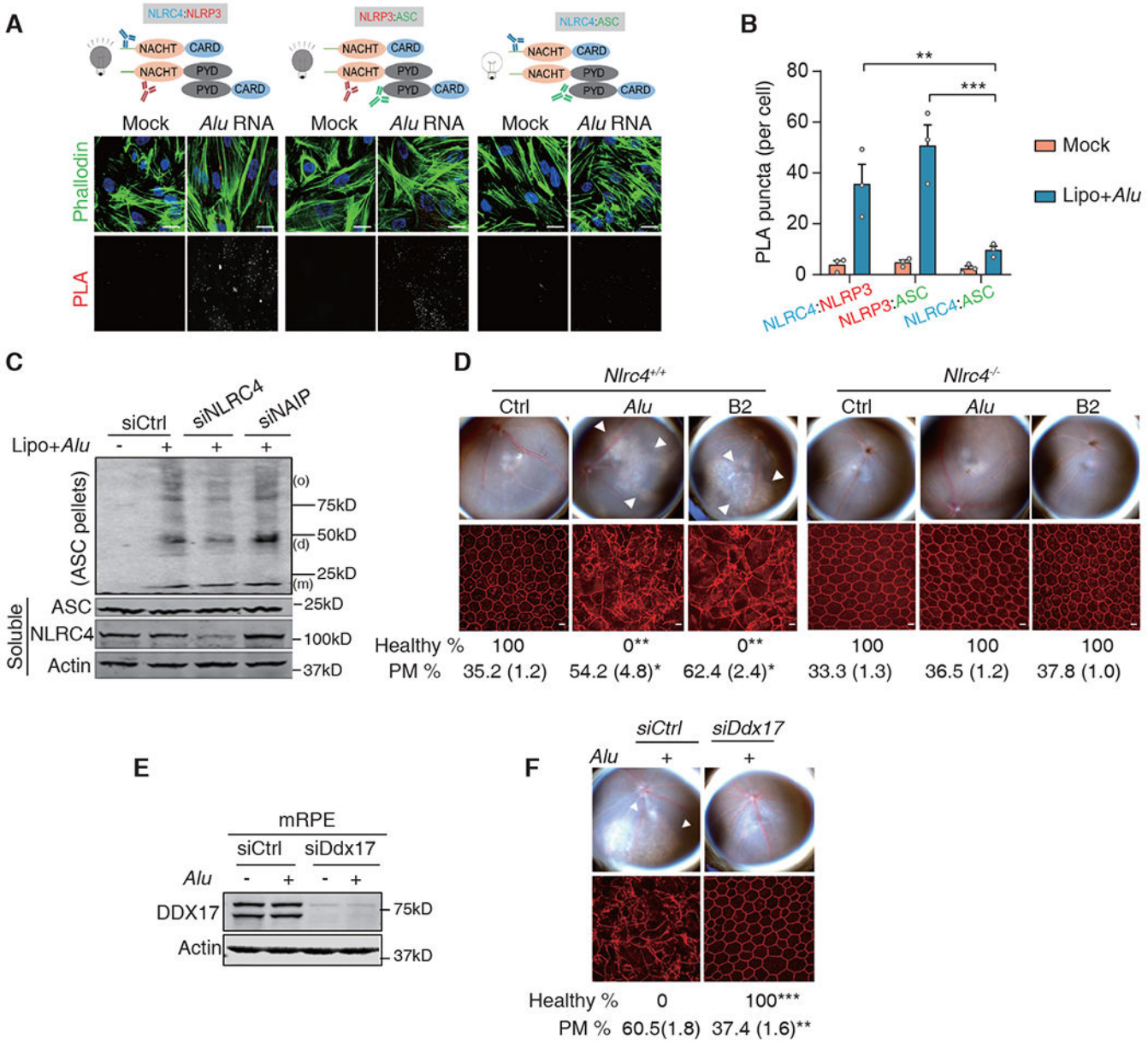

Fig. 6. SINE RNAs-induced RPE degeneration requires NLRC4.

(**A**) Confocal microscopy of RPE cells transfected with 100 pmol of *Alu* RNA or mock for 12 hours following proximity ligation assay (PLA) between NLRC4-NLRP3; NLRP3-ASC; NLRC4-ASC. The PLA labeled protein interaction sites (gray puncta); F-actin is labeled with Alexa Fluor™ 488 Phalloidin to visualize cell morphology. Scale bars, 20 μm. (**B**) Quantification of PLA puncta in human RPE cells transfected with 100 pmol of *Alu* RNA or mock. Shown is the mean ± SEM for independent experiments. $^{**}P < 0.01$; $^{***}P < 0.001$, two-way ANOVA with Sidak's multiple comparisons. (**C**) Immunoblot analysis of ASC and NLRC4 in cell lysates (soluble) and of ASC in DSS-crosslinked pellets (insoluble) in human RPE cells transfected with siRNAs (48 h) targeting NLRC4 or NAIP and transfected with 100 pmol of *Alu* RNA or mock. o, oligomers; d, dimers; m, monomers. (**D**) Fundus

photographs (top) and ZO-1–stained RPE flat mounts (bottom) of *Nlrc4*$^{+/+}$ and *Nlrc4*$^{-/-}$ mice treated with subretinal injection of vehicle (Ctrl), *Alu* RNA, or B2 RNA. Scale bars, 10 μm. Loss of regular hexagonal cellular boundaries represents degenerated RPE (outlined by white arrowheads). n = 5–6 (*Nlrc4*$^{+/+}$), n = 4–6 (*Nlrc4*$^{-/-}$) mice. (**E**) Immunoblot analysis of DDX17 and actin in primary mouse retinal pigment epithelium (mRPE) cells isolated from wild-type (WT) mice, transfected with *Ddx17* siRNA or control siRNA, followed by transfection with *Alu* RNA or mock. (**F**) Fundus photographs (top) and ZO-1-stained RPE flat mounts (bottom) of WT mice treated with subretinal injection of *Alu* RNA and intravitreous administration of *Ddx17* siRNA or control siRNA. Scale bars, 10 μm. Binary and morphometric quantification of RPE degeneration is shown (*$P < 0.05$; **$P < 0.005$). PM, polymegethism (mean (SEM)).